

POLITECNICO DI TORINO

Master's Degree
MECHATRONIC ENGINEERING

Master's Degree Thesis

**Modeling and simulation of a human walk with
foot-ground pressure analysis**



**Politecnico
di Torino**

Relatori

prof. Maurizio Morisio
prof. Giuseppe Menga

Candidato

Michela Rosati

Anno Accademico 2021-2022

*Ai miei genitori e a
nonna Tina.*

Summary

The thesis has a first introduction chapter, then is divided in two sections, a theoretical and a simulation part. For what concern the theoretical one:

- Second Chapter: in this section is explained the history of the walking robots (the chapter is done in collaboration with Gabriele Congedo).
- Third Chapter (Gait cycle): this section provides the reference system conventions (this subsection is done in collaboration with Gabriele Congedo), the cycles divisions and the gait phases and their detailed explanation, the definition of ZMP and 3D-LIPM (this subsection is done in collaboration with Gabriele Congedo). In this chapter there is also a summary of the work done by professor Menga.
- Fourth Chapter (Instrumentation): this section shows the instrumentation used in order to evaluate the human walk (the chapter is done in collaboration with Gabriele Congedo).
- Fifth Chapter (Biped design): in this section is explained how is done the biped design using sketch up and onshape.
- Sixth Chapter (theoretical study of kinematics): in this chapter the forward kinetics and the inverse one is done.

For what concern the simulation one:

- Seventh Chapter (Dataset): it describes the experimental datasets used in the various tests (the chapter is done in collaboration with Gabriele Congedo).
- Eighth Chapter (Simulation on Matlab): this section provides the data analysis, the ZMP and feet trajectories generation, the CoG computation, the direct and the inverse kinematics.

The last chapter is the Conclusion of the thesis in which I explained the pros and cons of my studies, they are a continuation of the studies done by previous colleagues.

Acknowledgements

Ringrazio il Prof. Maurizio Morisio e il Prof. Giuseppe Menga che mi hanno assistito nella ricerca e nel finalizzare il progetto.

Ringrazio Gabriele Congedo in quanto abbiamo parzialmente lavorato insieme al progetto.

Ringrazio i miei genitori che mi hanno sostenuto sempre, in ogni momento e per ogni scelta.

Ringrazio nonna Tina che con le sue parole mi ha sempre dato la forza e mi ha sempre messo il giusto umore. Ringrazio nonna Luisa e nonno Nicola che sono sempre stati nei miei pensieri. Ringrazio tutta la mia famiglia.

Ringrazio le mie amiche romane che mi hanno sempre supportato in questo percorso sia di studio che di vita.

Ringrazio Torino anche se tra noi c'è un odi et amo. Ringrazio tutte le persone conosciute in questi anni perchè senza di loro probabilmente sarebbe stato più difficile arrivare fino qui. Ringrazio soprattutto chi è riuscito a rendermi le giornate più leggere e chi, nonostante tutto, c'è sempre.

Contents

List of Tables	8
List of Figures	9
1 Introduction	11
I	13
2 History of walking robots	15
2.1 Walking Robots	15
2.2 Development of Exoskeletons	17
2.2.1 Periods of innovation	17
3 Gait Cycle	21
3.1 Reference systems conventions	21
3.2 Cycles Divisions	22
3.3 Gait Phases	24
3.4 Ankle-Foot, Knee, Hip analysis	26
3.4.1 Ankle-Foot	26
3.4.2 Knee	32
3.4.3 Hip	34
3.4.4 Total Limb	35
3.4.5 Simulation results	42
3.5 Defining the Measure of Balance	42
3.5.1 Zero Moment Point	42
3.6 Model for biped robots	50
3.6.1 Linear Inverted Pendulum Model (LIPM)	50
3.6.2 3D Linear Inverted Pendulum Model (3D-LIPM)	52
3.6.3 The cart-table model	54
3.6.4 The Spherical Inverted Pendulum	56
3.6.5 Final Considerations	57

4	Instrumentation	59
4.1	Non-wearable sensors	59
4.1.1	Force transducers and force plates	59
4.1.2	Treadmills	60
4.2	Wearable sensors	60
4.2.1	Optoelectronic stereophotogrammetry	60
4.2.2	Accelerometer	60
4.2.3	Gyroscope	61
4.2.4	Magnetometer	61
4.2.5	Inertial Measurement Units	61
4.2.6	Electrogoniometers	62
4.2.7	Optical fiber sensors	62
4.2.8	Textile-based sensors	63
4.2.9	EMG signals	63
5	Biped design	65
5.1	SketchUp	65
5.2	Onshape	66
6	Theoretical study of kinematics	69
6.1	Forward Kinematics	70
6.2	Inverse Kinematics	70
II		75
7	Dataset	77
7.1	Incline Experiment	77
8	Simulation on Matlab: data analysis and variables generation	87
8.1	Data analysis	87
8.2	Cartesian variables generation	94
8.2.1	ZMP and feet trajectories generation	94
8.2.2	CoG computation	97
8.3	Kinematic model	100
8.3.1	Direct kinematics	100
8.3.2	Inverse kinematics	101
8.4	Final results and considerations	104
III	Conclusion	107
9	Conclusion	109

List of Tables

3.1	Floor Contact Periods	23
3.2	Ankle motion	26
3.3	Knee motion	32
3.4	Hip motion	34
8.1	Chosen center offsets for the subject AB07 and trial s1i0	93

List of Figures

2.1	ASIMO	16
2.2	MAHRU	16
2.3	QRIO	16
2.4	WABIAN	16
2.5	Robert Seymour	17
3.1	Anatomical body planes and directions	22
3.2	Division of the gait cycle	23
3.3	A step versus a stride	24
3.4	Ankle motion: the black line is the mean, the dotted line is 1 standard deviation [16]	26
3.5	IC	27
3.6	LR	27
3.7	MSt	28
3.8	TSt	29
3.9	PSw	29
3.10	Arch-type skeletal structure of human foot	30
3.11	Transient pressure distribution on sole during a single stride (standard male)	31
3.12	Knee motion: the black line is the mean, the dotted line is 1 standard deviation [16]	32
3.13	Hip motion: the black line is the mean, the dotted line is 1 standard deviation [16]	34
3.14	IC	36
3.15	LR	37
3.16	MSt	38
3.17	TSt	39
3.18	PSw	39
3.19	ISw	40
3.20	MSw	41
3.21	TSw	41
3.22	Flexion-extension joint angles	42
3.23	The use of center of gravity as a measure of balance is only acceptable when the motions are slow and the dynamic forces are negligible.	44
3.24	Support foot and influence of by the force, moment, ground reaction	45

3.25	(a) dynamically balanced gait, (b) unbalanced gait where ZMP does not exist and the ground reaction force acting point is CoP while the point where $M_x = 0$ and $M_y = 0$ is outside the support polygon (FZMP). The system as a whole rotates about the foot edge and overturns, and (c) tip-toe dynamic balance	47
3.26	Foot of the supporting in the single-support phase	49
3.27	Rotation of the supporting foot about its edge.	49
3.28	Linear Inverted Pendulum Model	50
5.1	Biped design on SketchUp	66
5.2	Prototype created on Onshape	67
5.3	Kinematic chain on Simulink	68
6.1	Kinematic description of the robot legs	69
6.2	Sagittal Plane right leg	71
6.3	Frontal Plane	73
7.1	Continuous data Hierarchy	85
7.2	Gait cycle data Hierarchy	86
8.1	State machine	88
8.2	Heel and toe markers position along the axis z for the subject AB07 and trial s1i0. The minimum are highlighted with the circle	89
8.3	Relationship between two successive joint centers and related markers	90
8.4	Algorithm 1	92
8.5	Markers and body segments	93
8.6	Comparison between computed ZMP footprints and meta trajectories.	95
8.7	Comparison between the generated ZMP (black line) and the CoPs (blue and red lines) taken from experimental data along the lateral direction and the longitudinal lateral direction.	96
8.8	Comparison of the reference and tracked ZMP with the generated CoG along x and y	99
8.9	Comparison between CoG and ZMP on the xy ground plane	99
8.10	Initial contact phase	105
8.11	Loading response phase	105
8.12	Mid-stance phase	106
8.13	Swing phase	106

Chapter 1

Introduction

Robotics concerns the study of those machines that can replace human beings in the execution of a task, as regards both physical activity and decision making. Robotics is commonly defined as the science studying the intelligent connection between perception and action [7].

My thesis is organized in the following way:

- Theoretical part in which there is some history of robotics, an in-depth study on human locomotion, a presentation of what was used to collect the data used subsequently for the simulation, the creation of the biped used and the corresponding direct and inverse kinematics.
- Practical part in which there are the results of the simulation obtained using Matlab.

This thesis has the purpose to provide the design basis of a walking haptic exoskeleton for rehabilitation of the lower limbs. In particular, complete gait trials in order to better understand the lower limbs movements during walking. The postural equilibrium was evaluated using a stability criteria for the bipeds' gait, the zero moment point (ZMP) of Vukobratovic. To find out the link between the ZMP and the center of mass (CoM) trajectory is used the Kajita linear inverted pendulum model (LIMP), a robotics gait model.

Part I

Chapter 2

History of walking robots

In this first part of the thesis is presented the history of walking robots. This chapter is entirely done in collaboration with Congedo Gabriele [2].

2.1 Walking Robots

The development of a humanoid has been the focus of the robotics community in recent years. Many studies on biped walking robots have been performed since 1970. During that period, biped walking robots have transformed into biped humanoid robots through technological development. The strong focus on biped humanoid robots stems from a long-standing desire for human-like robot that is desirable for coexistence in a human-robot society [8]. Biped humanoid robot research groups developed their own robot platform and dynamic walking control algorithms. This has resulted in promising developments such as the ASIMO, Fig. 2.1, (the acronym of "Advanced Step In Mobility") humanoid robot, developed by HONDA with 32 DOF and 52 kg weight or the 62 kg MAHRU, Fig. 2.2, series of Samsung Electronics with 32 DOF. Further examples of contributions in the humanoid robots field are the QRIO, Fig. 2.3, which has an adaptable motion controller that allows the displacements on uneven surfaces and external forces and the WABIAN, Fig. 2.4, series of Waseda University with 35 DOF, which has played a fundamental role in the evolution of humanoid robots.



Figure 2.1. ASIMO



Figure 2.2. MAHRU

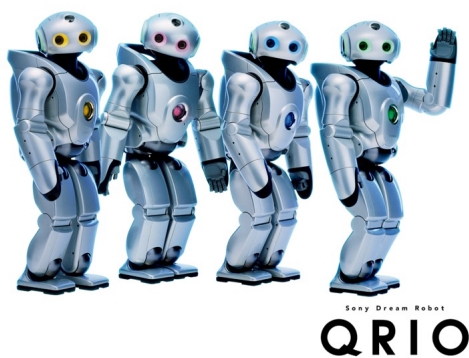


Figure 2.3. QRIO

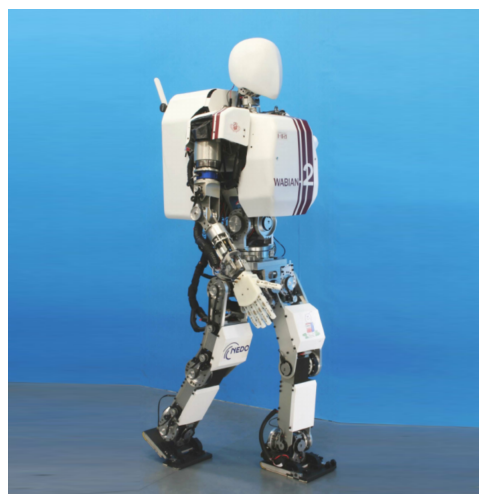


Figure 2.4. WABIAN

Some of the most studied architectures found in the literature include the H7 from the University of Tokyo with a total of 30 DOF, including one DOF toe joint. Another example is the JOHNNIE robot from the Technical University of Munich, where each leg incorporates six driven joints, three DOF in the hip, one DOF for the knee, and another two DOF for the ankle joint. Nowadays, most of the humanoid robots mentioned above consist of two 6-DOF legs, namely 3-DOF hip, 1-DOF knee and 2-DOF ankle. Although the efforts have mainly focused on achieving human gait, this feature has not been successfully accomplished with a limited number of DOF. Thus, it becomes necessary to incorporate redundant DOF in order to achieve an approximate human gait motion. The addition of an active toe joint to the kinematic model of each leg has drawn huge interest, because compared with conventional humanoid robots that are equipped with

flat feet, this architecture allows a robot to walk in a more natural way. There are several references in the literature related to toe joints in biped robots [9].

2.2 Development of Exoskeletons

The exoskeletons are generally regarded as a technology that extends, complements, substitutes or enhances human function and capability or empowers the human limb where it is worn. The operator of an exoskeleton is a human who needs to make decisions and perform tasks with exoskeletons, this is the principal difference from other robots. Combining human intelligence and machine power exoskeletons enhance the abilities of both human power and machine intelligence. Since the concept of exoskeleton was produced in the 19th century, the development of exoskeletons have undergone five phases, i.e. sprout period, exploration period, dormancy period, accumulation period and climax period. Exoskeletons apply and merge manifold techniques involving mechanical and electronic engineering, automation technology, biological, medical, and material science. Recently, exoskeletons are applied in military, civilian and rehabilitation.

2.2.1 Periods of innovation

Sprout period

The sprout period lasted more than one century from 1830 to 1960. During this period, a British inventor Robert Seymour proposed the concept to help people walk by a wearable device which was propelled by steam in 1830 Fig. 2.5. An American inventor Ira C.C.

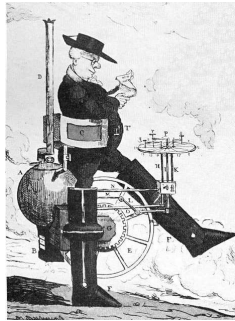


Figure 2.5. Robert Seymour

Rinehart conceptually designed a walking machine which enabled an individual to step seven feet and four inches at an ordinary stride in 1889. From 1889 to 1890, Nicholas Yagn, of St.Petersburg, Russia, designed walking, jumping, and running assisted devices using a giant leaf spring. In 1890, another inventor Yagn designed an exoskeleton with long leaf springs in parallel to the legs to help people run faster and jump higher. In the stance phase, the weight of the body can be transferred to the ground directly by the spring to reduce the forces on the standing leg. Most exoskeletons were conceptual designs in the sprout period due to the limitations of the technology at that time.

Exploration period

The exoskeleton HARDIMAN developed by the US Department and General Electric in 1965 marked the exoskeleton development entering the exploration period. HARDIMAN aimed at augmentation that the individual who wore it could lift 1,500 lbs (682kg). In fact, only one arm of HARDIMAN was developed and achieved to lift 750lbs (341kg) until the 1970s. The failure of HARDIMAN was mainly caused by the fact that the energy supplies were too huge to be portable, and the speed of data processing and function control was slow. In the late 1960s and 1970s, an active anthropomorphic exoskeleton with pneumatic power and partly cinematic program for paraplegics was developed at the Mihailo Pupin Institute under the Prof. Vukobratovic's guidance. At the same time, the theory of legged locomotion systems was first put forward by Prof. Vukobratovic, which established the foundation for present modern high-performance exoskeletons. The researchers of University of Wisconsin started to develop a full lower limb exoskeleton in 1968. This exoskeleton was designed to help those paraplegics with complete upper limb capabilities to walk again. The wearer can implement the sit-to-stand, stand-to-sit translation and walk at 50% of normal speed. Both hip and ankle joints had three rotational degrees of freedom (DOF) and the knee joint had one rotational DOF. The joints at hip and knee for flexion/extension were actuated by hydraulic power, and the other joints were passive.

Dormancy period

The development of exoskeleton entered the dormancy period in the 1980s. In the middle 1980s, the exoskeleton concept "Pitman" was put forward by Jeffrey Moore at the Los Alamos National Laboratory (Los Alamos, NM) to apply in the military to augment the soldiers' capabilities. However, this exoskeleton program was not funded by the U.S. Defense Advanced Research Projects Agency (DARPA). In 1988, Prof. Jichuan Zhang started to research the electric walking machine for high leg paraplegia patients at Tsinghua University. Using the bar linkage mechanism, the ipsilateral hip joint and knee joint of the exoskeleton were actuated by only one motor. This structure decreased the weight of the exoskeleton and became more compact and portable. In 1990, G. John Dick and Eric A. Edwards developed Spring-Walker according to the mechanism that a device in series with the human leg can reduce the metabolic cost of running by lowering impact losses and by providing energy return. However, Spring-Walker can only enhance jumping height. For running, it even increased metabolic cost by 20% compared to locomotion without it.

Accumulation period

From 1990 to 2000, the research of exoskeleton went into the accumulation period. In 1992, Prof. Yoshiyuki Sankai of University of Tsukuba started to develop a wearable type robot 'Robot Suit HAL' (Hybrid Assistive Limb), which was intended to physically support a wearer's daily activities and heavy work. The first prototype named HAL-1 adopted DC motors and ball screws to augment the wearer's joint torque. In 1994, researchers of Kanagawa Institute of Technology developed a wearable power assisting suit for nurses to enhance their muscle strength to lift patients and avoid back injuries. The movement of the joints at arms, waist and legs of the suit were sensed by strain sensors to detect the muscle force and actuated by pneumatic rotary actuators with concentric round boxes sliding each other. Compared to the over-ground exoskeletons, Hocoma AG developed

an immobile exoskeleton Lokomat consisting of an over-ground exoskeleton, an advanced body weight support system (BWS) and a treadmill in 2000 in Switzerland. The Lokomat with repetitive walking on one hand helps to improve circulation, strengthen bones and muscles and gain a natural walking pattern, on the other hand decrease the physical effort and constraint of the therapists.

Climax period

Exoskeletons attracted much more attention from researchers from different countries including US, Japan, Israel, France, Switzerland, South Korea, China, etc. and the development of exoskeletons went into the climax period since 2000. One representative of exoskeletons applied in the military, Berkeley Lower Extremity Exoskeleton (BLEEX) was developed to increase soldier's load capacity, lessen the risk of leg and back injury, decrease the metabolic consumption and reduce the perceived level of difficulty. BLEEX adopted the hybrid hydraulic-electric portable power supply in order to carry its own power source. The hip and ankle joint of BLEEX had three DOFs, respectively, among which hip flexion/extension, abduction/adduction and ankle flexion/extension were actuated by linear hydraulic actuators. Its knee joint had one DOF actuated for flexion/extension. The control system of BLEEX mainly collected sensory information from exoskeletons to determine the kinematic and dynamic parameters. It was reported that the soldier who wore BLEEX can walk at 0.9 m/s with load up to 75 kg and 1.3 m/s without load. The representative civil application of exoskeletons was the Robot Suit Hybrid Assistive Limb (HAL)-5 developed by Professor Yoshiyuki Sankai at University of Tsukuba for both power augmentation and walk assistance. The hip and ankle joint of HAL-5 were actuated by a DC motor with harmonic drive for flexion/extension, respectively, and the ankle joint for flexion/extension DOF was passive with springs to return a normal angle. HAL-5 adopted joint torque augmentation at the hip, knee and ankle joint, which is different from BLEEX transferring the load to ground. HAL-5 had two types of control systems: "Cybernic Voluntary Control System" and "Cybernic Autonomous Control System". Cybernic Voluntary Control System understood the wearer's voluntary intention according to the surface electromyographic (sEMG) signals through placing the sEMG electrodes below the hip and above the knee. Then the power units of HAL-5 generated power assist torque by amplifying the wearer's joint torque estimated from EMG signals. Cybernic Autonomous Control System was developed to provide effective physical supports for the handicaps by the potentiometer, ground reaction force sensors, a gyroscope and accelerometer on the backpack to estimate the posture since the signals of handicaps could cause a broken walking pattern. ReWalk from Argo Medical Technologies has been commercialized for fundamentally changing the health and life experiences of individuals with spinal cord injuries (SCI). It consisted of a wearable brace support suit with DC motors at hip and knee joint, respectively, rechargeable batteries, a computer-based controller contained in a backpack, a wireless mode selector, and an array of sensors that measure upper body tilt angle, joint angles, and ground contact. ReWalk utilized a closed-loop algorithm software control and triggered and maintained the walking pattern by detecting the wearer's upper-body movements. Additionally, ReWalk can also help the wearer climb stairs, transform from sitting to standing and vice versa. The crutches were necessary to keep balance [10].

Chapter 3

Gait Cycle

In order to understand the human walking there are three basic approaches [16]:

- First: The simplest system subdivides the cycle according to the variations in reciprocal floor contact by the two feet.
- Second: This method uses the time and distance qualities of the stride.
- Third: It identifies the significant events within the gait cycle and designates these intervals as the functional phases of gait.

3.1 Reference systems conventions

This section is entirely done in collaboration with Congedo Gabriele [2].

In order to keep track of all the kinematic variables (linear and angular displacements, velocities and accelerations), it is important to establish the convention systems in which they represent them. The first thing is to establish an absolute spatial reference system. The one utilized is based on the body planes, hypothetical geometric planes used to divide body into sections, used in anatomical terminology Fig. 3.1.

Three planes can be defined:

- **Frontal plane** is the vertical plane dividing the body in anterior and posterior part.
- **Trasversal or medial plane** is horizontal, and splits the body in the upper and lower part.
- **Sagittal plane** is vertical, and separates the body in the left and right part.

The axis of the reference system are X in the direction of progression at the intersection of the sagittal and transverse planes, it is positive in the anterior direction; Y in the sideways direction at the intersection of the transverse and frontal plane, it is positive in the left direction; Z in the vertical direction at the intersection of the transverse and frontal plane, it is positive in the superior direction. The origin of this absolute reference system is located on the body center of gravity or of mass (CoG or CoM). In some cases

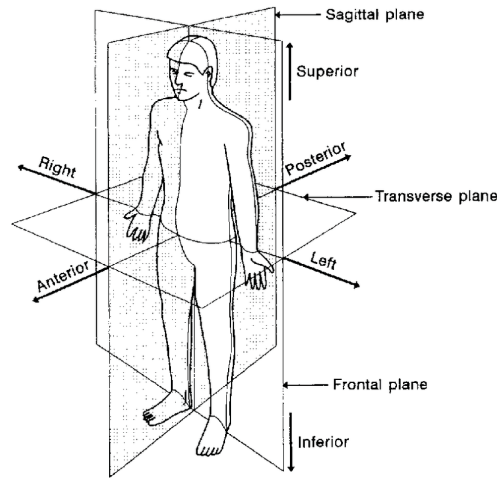


Figure 3.1. Anatomical body planes and directions

it has been useful to represent the kinematic variables not w.r.t. to the center of mass, but w.r.t. the ground. The new reference system will have as its center the projection of the CoG on the ground, and the XY plane will no longer correspond to the medial plane but to the ground surface. Joint angular displacements and velocities are expressed w.r.t. a local frame, centered in the center of the articulation. It has as its axis the axis of joint rotation, an axis directed along one of the body segments connected by the joint and the last one positioned according to the right hand rule.

Three principal movement can be defined:

- **Flexion and extension:** for joint rotations in the sagittal plane. In particular, flexion: the articulation angle is decreasing; extension the articulation angle increases.
- **Abduction and adduction:** for joint rotations in the frontal plane. During abduction the body segment is moved away from the medial line, and in the adduction the opposite occurs.
- **External and external rotation:** rotations of a limb around its axis on the horizontal plane. In the former brings the limb closer to the medial line, in the latter further.

3.2 Cycles Divisions

Each gait cycle (GC) is divided into two periods or gait phases [16], as in Fig. 3.2:

- **Stance:** the entire period during which the foot is on the ground, it begins with initial contact. In particular, the stance is subdivided into three intervals: the start and the end involve a period of double stance (bilateral foot contact with the floor), while the middle portion has one foot contact (single stance).

- Swing: the time in which the foot is in the air for limb advancement, it begins as the foot is lifted from the floor, also known as toe-off.

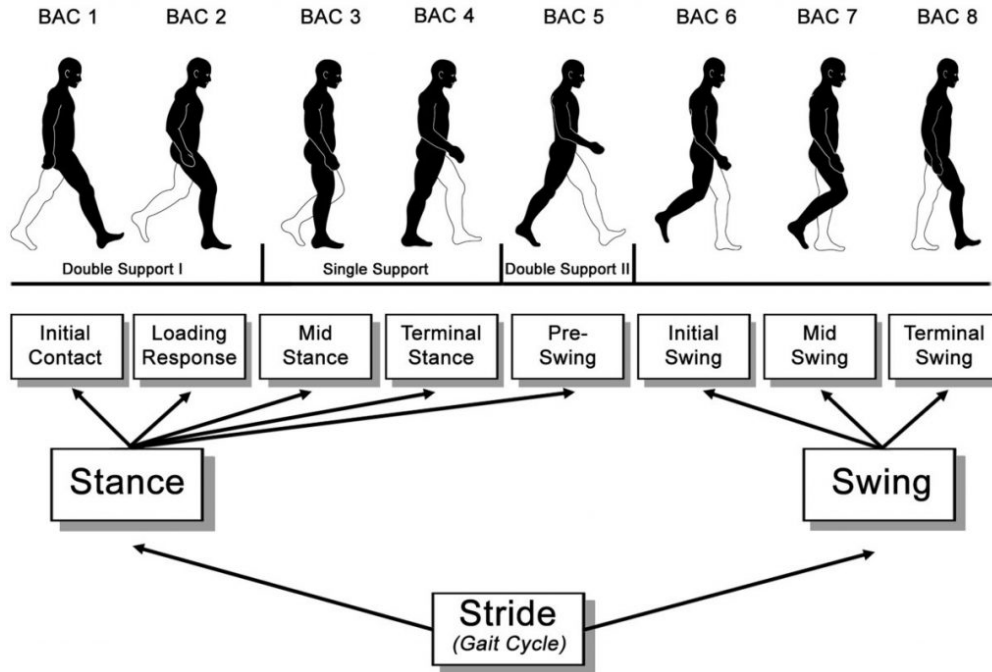


Figure 3.2. Division of the gait cycle

The gross normal distribution of the floor contact periods is 60% for stance and 40% for swing Table 3.1. Timing for the phases of stance is 10% for each double stance interval

Stance	60%
Initial Double Stance	10%
Single Limb Support	40%
Terminal Double Stance	10%
Swing	40%

Table 3.1. Floor Contact Periods

and 40% for single limb support. Note that single limb support of one limb equals swing of the other, as they are occurring at the same time. The precise duration of these gait cycle intervals varies with the person’s walking velocity. The duration of both gait periods shows an inverse relationship to walking speed. That is, both total stance and swing times are shortened as gait velocity increases. The change in stance and swing times becomes progressively greater as speed slows. Among the subdivisions of stance a different relationship exists. Walking faster proportionally lengthens single stance and

shortens the two double stance intervals.

The reverse is true as the person's walking speed slows. This pattern of change also is curvilinear. Having an interval when both feet are in contact with the ground for the limbs to exchange their support roles is a basic characteristic of walking. When double stance is omitted, the person has entered the running mode of locomotion [16].

The gait cycle also has been identified by the descriptive term stride. Occasionally the word step is used, but this is inappropriate, in Fig. 3.3. Stride is the equivalent of a gait cycle. It is based on the actions of one limb. The duration of a stride is the interval between two sequential initial floor contacts by the same limb (i.e., right IC and the next right IC). Step refers to the timing between the two limbs. There are two steps in each stride (or gait cycle). At the midpoint of one stride the other foot contacts the ground to begin its next stance period. The interval between an initial contact by each foot is a step (i.e., left and then right). The same offset in timing will be repeated in reciprocal fashion throughout the walk [16].

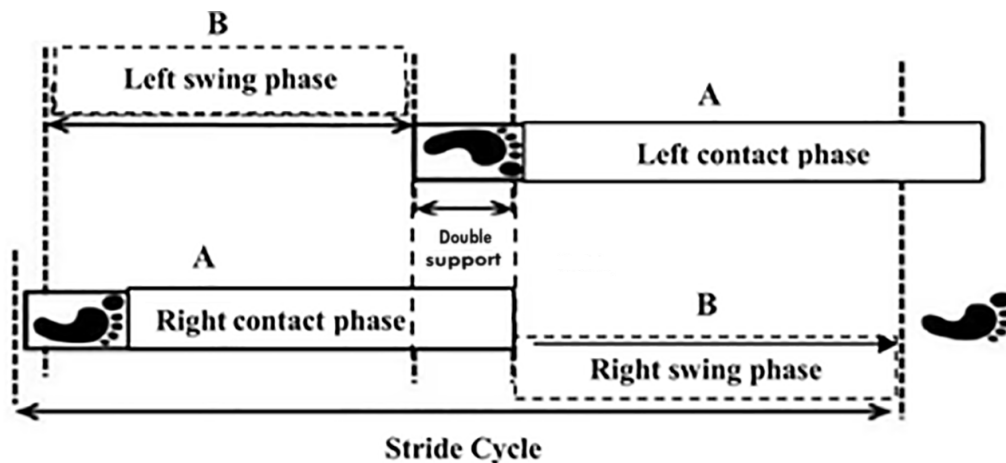


Figure 3.3. A step versus a stride

3.3 Gait Phases

For Perry [16], the gait cycle can be split in more refined sub-phases depending on the support phases and the task which is being executed, in Fig. 3.2.

- **Task: Weight acceptance**

- *Phase 1 - Initial Contact (IC):*

Interval: 0-2% GC.

It includes the moment when the foot, in particular the heel, just touches the floor. The joint postures present at this time determine the limb's loading response pattern.

Objectives: the limb is positioned to start stance with a heel rocker.

– *Phase 2 - Loading Response (LR):*

Interval: 0-10% GC.

It is the initial double stance period. The phase begins with initial floor contact and continues until the other foot is lifted for swing.

Objectives: shock absorption, weight-bearing stability and preservation of progression.

• **Task: Single Limb Support**

– *Phase 3 - Mid Stance (MSt):*

Interval: 10-30% GC.

It is the first half of the single limb support interval. It begins as the other foot is lifted and continues until body weight is aligned over the forefoot.

Objectives: progression over the stationary foot, limb and trunk stability.

– *Phase 4 - Terminal Stance (TSt):*

Interval: 30-50% GC.

It completes single limb support. It begins with heel rise and continues until the other foot strikes the ground. Throughout this phase body weight moves ahead of the forefoot.

Objectives: progression of the body beyond the supporting foot.

• **Task: Limb advancement**

– *Phase 5 - Pre-Swing (PSw):*

Interval: 50-60% GC.

It is the final phase of stance and is the second double stance interval in the gait cycle. It begins with initial contact of the opposite limb and ends with ipsilateral toe-off.

Objectives: position the limb for swing

– *Phase 6 - Initial Swing (ISw):*

Interval: 60-73% GC.

It is approximately one-third of the swing period. It begins with lift of the foot from the floor and ends when the swinging foot is opposite the stance foot.

Objectives: foot clearance of the floor and advancement of the limb from its trailing position.

– *Phase 7 - Mid Swing (MSw):*

Interval: 73-87% GC.

It begins as the swinging limb is opposite the stance limb. The phase ends when the swinging limb is forward and the tibia is vertical (i.e., hip and knee flexion postures are equal).

Objectives: limb advancement and floor clearance from the floor.

– *Phase 8 - Terminal Swing (TSw):*

Interval: 87-100% GC.

It begins with a vertical tibia and ends when the foot strikes the floor. Limb advancement is completed as the leg (shank) moves ahead of the thigh.

Objectives: complete limb advancement and prepare the limb to stance.

3.4 Ankle-Foot, Knee, Hip analysis

This analysis is taken from [16].

3.4.1 Ankle-Foot

Ankle-Foot motion

Terminology:

- Dorsiflexion: upward travel of the foot.
- Planar flexion: downward motion of the foot.

In the Fig. 3.4 is present the entire range of ankle motion used during the walking. In order to understand the motion during a stride the following table is used:

Planar flexion to 7°	0-12% GC
Dorsiflexion to 10°	12-48% GC
Planar flexion to 20°	48-62% GC
Dorsiflexion to neutral	62-100% GC

Table 3.2. Ankle motion

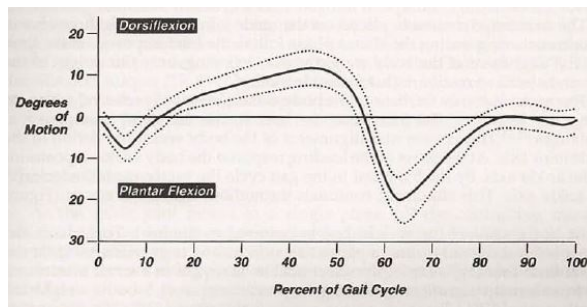


Figure 3.4. Ankle motion: the black line is the mean, the dotted line is 1 standard deviation [16]

Lets analysed the ankle function by gait phase (Fig. 3.2):

- **Task: Weight acceptance**

- *Phase 1 - Initial Contact (IC):*

- Posture: Ankle at 90° (neutral) to initiate a heel rocker.

- Function: heel rocker. The initial impact vector is vertical, this means that the forces are directed into the floor, Fig. 3.5.

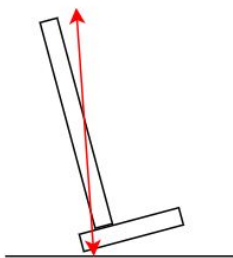


Figure 3.5. IC

- *Phase 2 - Loading Response (LR):*

- Motion: first arc of ankle planar flexion

- Function: heel rocker. The initial impact vector is vertical, this means that the forces are directed into the floor, Fig. 3.6. This provides stability.

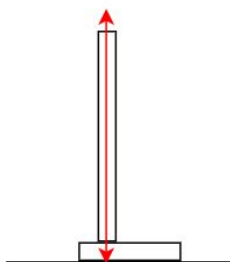


Figure 3.6. LR

- **Task: Single Limb Support**

- *Phase 3 - Mid Stance (MSt):*

- Motion: first arc of ankle dorsiflexion

- Function: ankle rocker for progression.

Throughout mid stance the body vector advances across the foot in response to momentum from the swing limb and forward fall of body weight, Fig. 3.7.

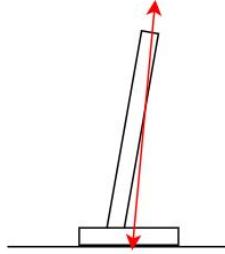


Figure 3.7. MSt

– *Phase 4 - Terminal Stance (TSt):*

Motion: heel rise with continued ankle dorsiflexion

Function: forefoot rocker for progression.

By the end of the mid stance the base of the body vector lies in the forefoot, Fig. 3.8. With the body vector based in the area of the metatarsal heads the dorsiflexion lever is the full length of the forefoot. This, combined with the falling of body weight, generates a maximal dorsiflexion torque at the ankle. In this phase the heel rises, this means that the body weight must be supported, thus there is a demand for strong soleus action. The combination of ankle dorsiflexion and heel rise in TSt places the body's center of gravity anterior to the source of foot support. As the center of pressure moves more anterior to the metatarsal head axis, the foot rolls with the body. The effect is an ever-increasing dorsiflexion torque. This creates a free forward fall situation. As forward roll and downward fall are combined, a force is created against the floor. By the end of TSt, advancement of the base of the body vector to the metatarsal joints and the forward fall has progressed to a state where there is no available restraint. Also, there is no stabilization force within the foot. Terminal stance is ended by the other foot contacting the floor to reestablish stability.

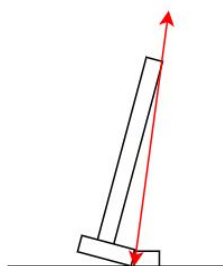


Figure 3.8. TSt

- **Task: Limb advancement**

- *Phase 5 - Pre-Swing (PSw):*

Motion: second arc of ankle planar flexion

Function: initiate knee flexion for swing.

In this phase continued floor contact assists body balance as body weight is transferred to the other limb, while the synergy of muscle action and ankle motion are the primary factors in initiating swing, Fig. 3.9.

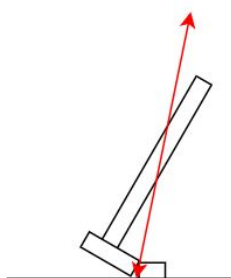


Figure 3.9. PSw

- *Phase 6 - Initial Swing (ISw):*

Motion: initiation of the second arc of dorsiflexion

Function: floor clearance for limb advancement.

- *Phase 7 - Mid Swing (MSw):*

Motion: continued ankle dorsiflexion

Function: floor clearance.

- *Phase 8 - Terminal Swing (TSw):*

Motion: support of the ankle at neutral

Function: prepare for IC.

In conclusion the most critical event is the gradual dorsiflexion that progresses through mid and terminal stance together with the heel rise at the onset of terminal stance [16].

Foot

This part is entirely done in collaboration with Congedo. Gabriele [2].

In human walking motion, the two feet play a crucial role in absorbing impact from the ground, maintaining stability on uneven soil, and helping turning motions. In the same way, the critical design consideration with the foot of a bipedal robot is to enhance walking stability and performance. The study of the robotic foot purpose is to implement a human-like walking motion for biped robots by applying the characteristics of the human foot to the mechanism design. There has been a recent trend in foot design of adopting simple toe and heel joints to follow human ankle motion in landing on and taking off from the ground. First of all, it was confirmed that the flexible foot with toe joints enables increased walking speed and step length and it reduces energy consumption compared with flat feet. Along with the mechanical design of the flexible foot, a well-planned walking pattern is required in order to achieve human-like motion. It has also been found that the foot trajectory pattern with heel-contact and toe-off motion produces a smoother hip trajectory and increases adaptability to rough terrains. These works suggest that adopting toes and heels in the design of the foot mechanism is of great benefit in enhancing the performance and stability of bipedal robots. However, most of these approaches are not matured yet and are lacking in analytical considerations for determining design parameters. Hence, in terms of an anatomical and kinesiological analysis of the human foot, this section will investigate how to determine some critical foot parameters from the point of view of walking stability. In biomechanics, the functional efficiency of the human foot mechanism to support weight and absorb ground impact has been well investigated. As shown in Fig. 3.10 the human foot has an arch-type skeletal structure which connects heel, toes, and ankle, where the large bone at the heel called calcaneus supports about one third of the load and the metatarsal bones connected to the toes absorb the other impact force from the ground. The flexible tendon on the sole called the plantar fascia ligament is in charge

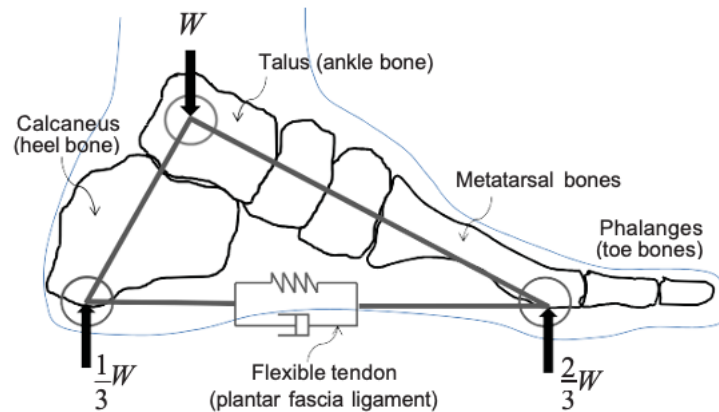


Figure 3.10. Arch-type skeletal structure of human foot

of the structural damping with the movement of the bones by varying the distance between heel and toe. It is also known that the division of toes helps to maintain stability while

walking during the stance phase by effectively distributing loads. In the mechanical design of a robot foot, more than that the human foot brings from a mechanical point of view. In particular, going into more specifics, there are three major articulations (joints) within the foot [16]:

- Subtalar (ST): junction between the talus and calcaneus.
- Midtarsal (MT): junction between the hind and forefoot.
- Metatarsophalangeal (MP): it is the toe break which allow the foot to roll over the metatarsal heads rather than the tips of the toes. The five metatarsal heads provide a broad area of support across the forefoot. In addition, the proximal phalanges allow an adjustable lengthening of the forefoot for progressional stability as needed.

During the walking motion, the sole of a human foot experiences pressure change due to the weight and ground reaction. The sole of a human foot mainly consists of three parts: heel part, toe joints (the part where the metatarsal bones end) and the five toes. Fig. 3.11 displays the pressure transition on the sole during a single stride by a standard male as the ZMP is moving forward from the heel to the toe. As shown, the largest pressure is exerted at the heel when the foot strikes the ground. The frontal big toe accepts much more pressure than others when the foot takes off from the ground, which is a reasonable result considering that the center of mass of the human body is located between the two feet [11]. To build a proper kinematic model of an human-exoskeleton

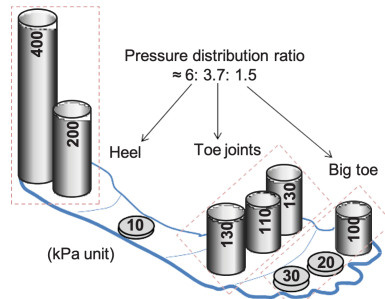


Figure 3.11. Transient pressure distribution on sole during a single stride (standard male)

system, human dimensions and have to be taken in account as a reference. Kinetics analyses also require data regarding mass distributions, mass centers, moments of inertia, and the like. It is also necessary to identify the exact location of the body joints centers of rotation. Anthropometry is the major branch of anthropology that studies the physical measurements of the human body to determine differences in individuals and groups. It relates the body characteristics described above with some of their determinants such as race, sex, age and body type, thanks to a wide variety of measurements. Dempster and coworkers (1955,1959)[13] have summarized estimates of segments lengths and joint center locations relative to anatomical landmarks. Drillis and Continini (1966) [14] reported an average set of segment lengths expressed as a percentage of the body total height, used as

relative unit of measure. By reasoning in this manner, they also computed the position of the center of mass of each body segment, and expressed it as a percentage of the total length of the segment. These segment proportion could be useful as a good approximation in absence of more accurate data, better if measured directly from the individual (Winter D., [12]). The moments of inertia of the body segment are defined about an axis of rotation which, in most studies, is passing through its center of gravity. Occasionally are defined as passing through an estimated joint center of rotation.

3.4.2 Knee

The knee is the junction between femur and tibia. Knee mobility and stability are the major factors in the normal pattern of walking [16]. In the Fig. 3.12 is present the entire range of knee motion used during the walking. In order to understand the motion during a stride the following table is used:

Flexion to 18°	0-15% GC
Extension to 5°	15-40% GC
Flexion to 65°	40-70% GC
Extension to 2°	70-97% GC

Table 3.3. Knee motion

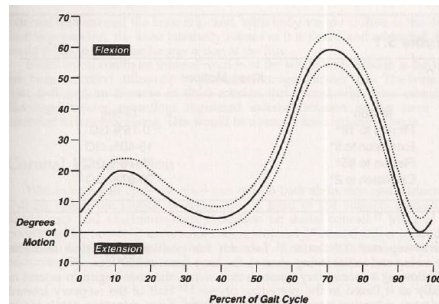


Figure 3.12. Knee motion: the black line is the mean, the dotted line is 1 standard deviation [16]

- **Task: Weight acceptance**

- *Phase 1 - Initial Contact (IC):*

Motion: Extended knee posture.

Functions: Stabilization weight-bearing.

Control: Anterior and posterior stabilization by the quadriceps and hamstrings, the anterior vector presents an extensor torque.

- *Phase 2 - Loading Response (LR)*:
Motion: Knee flexion (15°).
Functions: Shock absorption.
Control: Quadriceps extension versus the posterior vector, hamstring activity is waning.

- **Task: Single Limb Support**

- *Phase 3 - Mid Stance (MSt)*:
Motion: Knee extension.
Functions: Stable weight bearing.
Control:
 - * Early: Quadriceps continues
 - * Late: Passive extension by an anterior torque over a tibia stabilized by the soleus.
- *Phase 4 - Terminal Stance (TSt)*:
Motion: Completion of knee extension.
Functions: Stable weight bearing, further stride length.
Control: Passive extensor vector over a tibial stabilized by a soleus, at the end of the phase advancement of the tibia and foot moves the knee axis anterior to the vector, initiating flexion.

- **Task: Limb advancement**

- *Phase 5 - Pre-Swing (PSw)*:
Motion: Passive knee flexion.
Functions: Prepare for swing.
Control: Excessive passive flexion restrained by rectus femoris.
- *Phase 6 - Initial Swing (ISw)*:
Motion: Knee flexion.
Functions: Foot clearance for limb advancement.
Control: Flexion augment by forward thigh momentum.
- *Phase 7 - Mid Swing (MSw)*:
Motion: Passive knee extension.
Functions: Limb advancement.
Control: Passive extension as flexors relax and thigh advances.
- *Phase 8 - Terminal Swing (TSw)*:
Motion: Knee extension.
Functions: Complete step length (limb advancement), prepare for stance.
Control: Quadriceps activity to complete knee extension.

3.4.3 Hip

The hip is the junction between passenger and locomotor units [16]. In the Fig. 3.13 is present the entire range of hip motion used during the walking. In order to understand the motion during a stride the following table is used:

Flexion to 30°	0% GC
Flexion to 35°	85% GC
Extension to 10°	10% GC

Table 3.4. Hip motion

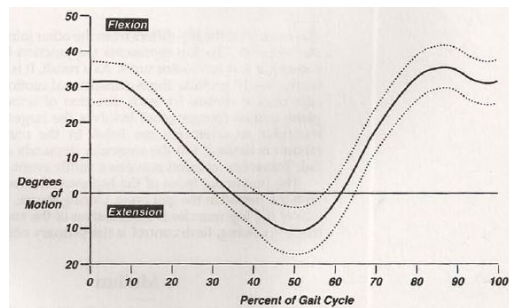


Figure 3.13. Hip motion: the black line is the mean, the dotted line is 1 standard deviation [16]

- **Task: Weight acceptance**

- *Phase 1 - Initial Contact (IC):*

Posture: Hip flexion at 30° (thigh forward).

IC hip extensor muscle action restrains flexor momentum, hamstrings muscles and gluteus maximus active.

- *Phase 2 - Loading Response (LR):*

Action: Sagittal and coronal positions are maintained.

LR hip extensor action; vector close to hip and posterior to knee; hamstring action reduced, gluteus maximus activity increased.

- **Task: Single Limb Support**

- *Phase 3 - Mid Stance (MSt):*

Action: Progressive hip extension.

MSt needs no hip extensor control as vector posterior to hip joint, gluteus medius coronal plane control still active.

- *Phase 4 - Terminal Stance (TSt):*

Action: Hyperextension of the hip.

- **Task: Limb advancement**

- *Phase 5 - Pre-Swing (PSw):*
Action: Hip flexion to neutral.
PSw hip flexion being initiated by adductor longus and rectus femoris, vector posterior to knee and at hip axis.
- *Phase 6 - Initial Swing (ISw):*
Action: Hip flexion.
ISw hip control with flexion being stimulated by iliacus muscle.
- *Phase 7 - Mid Swing (MSw):*
Action: Continuing hip flexion.
- *Phase 8 - Terminal Swing (TSw):*
Action: Cessation of hip flexion.
TSw cessation of hip flexion by hamstring muscle action.

3.4.4 Total Limb

In this subsection function at each joint has been detailed [16].

- **Task: Weight acceptance**

- *Phase 1 - Initial Contact (IC):*
Interval: 0-2% GC
Critical event: the most critical event in this phase is the floor contact by the heel, to initiate an optimum heel rocker, the ankle is at neutral, knee extended and hip flexed.

When the foot strikes the ground, the limb is optimally positioned to initiate both progression and knee stability. The ankle is in neutral dorsiflexion, the knee extended and the hip flexed (30°). The impact with the floor creates a momentary vertical floor reaction. At the ankle, the vector with its base in the heel creates a torque that opposes the ankle's dorsiflexion position. The knee is provided passive stability by the anterior alignment of the vector. Both the hip and trunk experience flexor torques due to the anterior location of the vector.

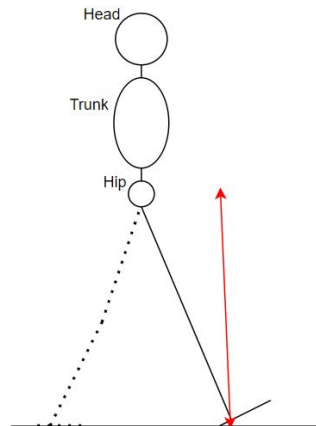


Figure 3.14. IC

– *Phase 2 - Loading Response (LR):*

Interval: 0-10% GC

Critical events:

- * Restrained knee flexion: shock absorption is provided by the quadriceps limiting the arc of knee flexion.
- * Restrained ankle planar flexion: the heel rocker continues body progression, while also contributing to shock absorption.
- * Hip stabilization: an erect posture of the trunk is preserved.

LR is the phase of greatest muscular activity since the three arcs of motion, which accompany limb loading, provide shock absorption to decrease the effect of rapid weight transfer. These actions are knee flexion to 18° , ankle planar flexion to 10° and subtalar valgus. All are stimulated by the body weight vector being located in the heel. At the same time, motion at the hip is minimized to stabilize the trunk over the weight accepting limb.

Sagittal plane motions are initiated by the heel rocker. Transfer of body weight onto the stance limb, with the heel as the only area of support, drives the forefoot toward the floor. The resulting motions are the ankle planar flexion and knee flexion.

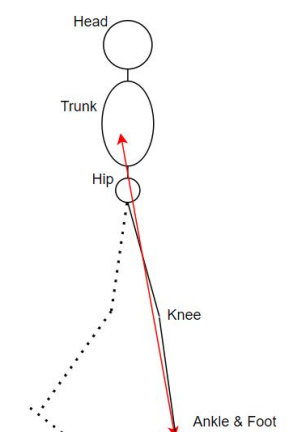


Figure 3.15. LR

- **Task: Single Limb Support**

- *Phase 3 - Mid Stance (MSt):*

Interval: 10-30% GC

Critical events:

- * **Restrained ankle dorsiflexion:** The ankle rocker motion allows forward progression.
- * **Knee extension:** Progressive straightening of the knee increases weight-bearing stability of the limb.
- * **Hip stabilization in the frontal plane:** Abductor muscle action stabilizes the pelvis in a level posture. This provides an appropriate base for an upright alignment of the trunk.

This phase is the time when the body weight line changes its anterior/posterior alignments at each joint. As the limb rolls forward over the supporting foot, the critical site for dynamic stability shifts from the knee to the ankle. During mid stance, the vector becomes anterior to the ankle and knee, and posterior to the hip. Contralateral toe-off transfers total body weight to the mid stance limb.

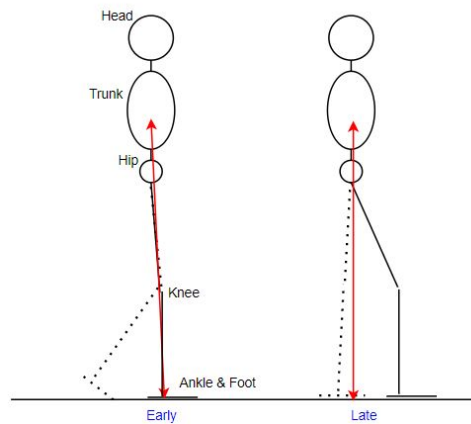


Figure 3.16. MSt

– *Phase 4 - Terminal Stance (TSt):*

Interval: 30-50% GC

Critical events:

- * Heel rise: The forefoot rocker allows body weight to advance beyond the area of support. Dynamic stabilization of the ankle is an essential element of heel rise.
- * Free forward fall of the body: This is the major component of progression. It also creates instability in sagittal plane balance.

As the body rolls forward over the forefoot, the ankle dorsiflexes to 10° and the heel rises as the knee completes its extension and the thigh reaches a trailing alignment. Advancement of the trunk moves the vector to its most anterior alignment at the ankle and the trailing posture of the limb allows body weight to drop at an accelerated rate that increases the vertical ground reaction force. The result is a large ankle dorsiflexion torque. Stability at the knee and hip is gained passively from the actions of the soleus on the tibia.

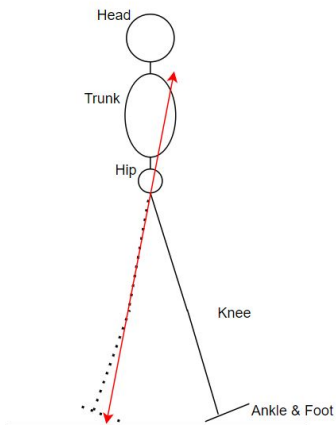


Figure 3.17. TSt

- **Task: Limb advancement**

- *Phase 5 - Pre-Swing (PSw):*

- Interval: 50-60% GC

- Critical events: the most critical event in this phase is the knee flexion.

- The large arc of knee flexion that will be needed in swing is initiated during this phase of double limb support. As the ankle planar flexes 20° , there is 40° knee flexion and hip flexion to neutral. Advancement of the vector to the metatarsophalangeal joint and unloading of the limb by weight transfer to the other toe causing a high heel rise.

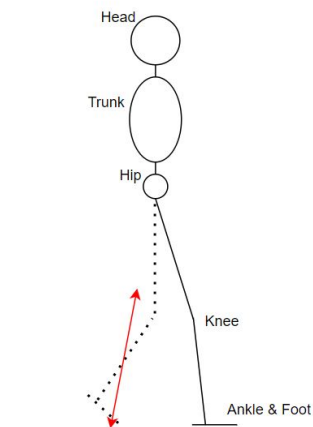


Figure 3.18. PSw

– *Phase 6 - Initial Swing (ISw):*

Interval: 60-73% GC

Critical events:

- * Knee flexion: the foot rises from the floor and it is dependent on adequate knee flexion.
- * Hip flexion: this is because there is a rapid advancement of the thigh.

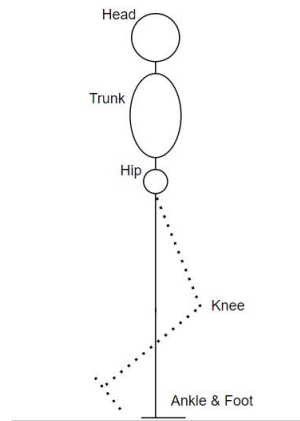


Figure 3.19. ISw

– *Phase 7 - Mid Swing (MSw):*

Interval: 70-85% GC

Critical events:

- * Ankle dorsiflexion: active control of the ankle enables the foot to clear the floor.
- * Hip flexion: limb advancement.

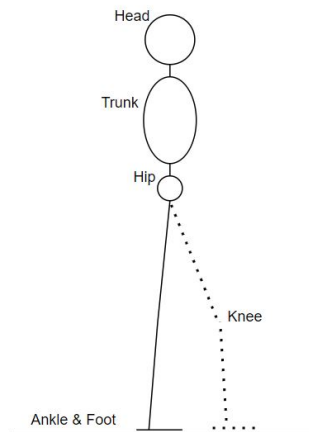


Figure 3.20. MSw

– *Phase 8 - Terminal Swing (TSw):*

Interval: 85-100% GC

Critical events:

- * Hip deceleration.
- * Knee deceleration.
- * Knee extension: this provides a position of passive knee stability in preparation for floor contact.
- * Ankle dorsiflexion: a neutral position is maintained to put the foot in the desired position for floor contact.

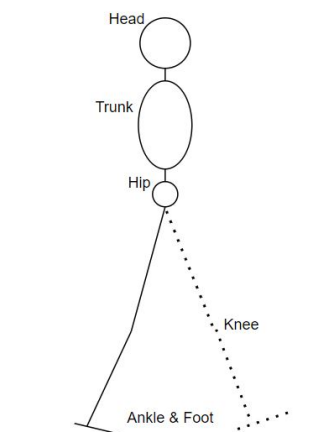


Figure 3.21. TSw

3.4.5 Simulation results

The ankles, knees, and hips articulations motion generate the gait. Each one possesses a certain number of degrees of freedom (dof). Joint angles can be represented either w.r.t. the time or w.r.t. the gait cycle percentage. The latter allows the evaluation of events during a single cycle, highlighting their dependence on angles. In Fig.3.22 are reported the ankle, knee and hip flexion-extension joint angles (X) w.r.t the gait cycle percentage of the subject AB07 in a plane treadmill trial belonging to the datasets [15]. In each plot the black line represents the mean angle, while the green lines are the various gait cycles angles.

This simulation results can be compared with Figs. 3.4, 3.12 and 3.13 taken from [16].

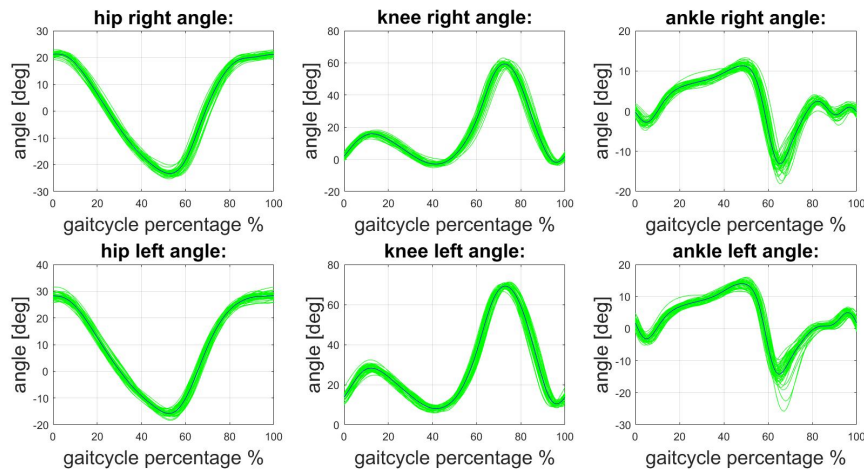


Figure 3.22. Flexion-extension joint angles

3.5 Defining the Measure of Balance

This section is partially done in collaboration with Congedo Gabriele [2].

The most important task to be considered during motion is the dynamic balance. The main parameters evaluated in the balance of a biped have been the center of pressure (CoP) and the Zero-Moment Point (ZMP) introduced by Vukobratovic [39]

3.5.1 Zero Moment Point

Zero moment point (ZMP) is a concept related to dynamics and control of legged locomotion. It specifies the point with respect to which dynamic reaction force at the contact of the foot with the ground does not produce any moment in the horizontal direction. The concept assumes the contact area is planar and has sufficiently high friction to keep the feet from sliding. This notion was introduced in January 1968 by Miomir Vukobratovic

at The Third All-Union Congress of Theoretical and Applied Mechanics in Moscow.

Comparison between ZMP, CoP and CoG

The zero moment point is a very important concept in the motion planning for biped robots. Since biped robots have only two points of contact with the floor and they are supposed to walk, “run” or “jump” (in the motion context), their motion has to be planned concerning the dynamical stability of their whole body. This is not an easy task, especially because the upper body of the robot (torso) has larger mass and inertia than the legs which are supposed to support and move the robot. This can be compared to the problem of balancing an inverted pendulum. The trajectory of a walking robot is planned using the angular momentum equation to ensure that the generated joint trajectories guarantee the dynamical postural stability of the robot, which usually is quantified by the distance of the zero moment point in the boundaries of a predefined stability region. The position of the zero moment point is affected by the referred mass and inertia of the robot’s torso, since its motion generally requires large angle torques to maintain a satisfactory dynamical postural stability [17]. Hence, ZMP is a measure of balance, not a control methodology. One of the most basic measures of balance is the vertical projection of the center of mass (COM) also known as the center of gravity (COG). If the system moves slowly enough, the dynamic forces are negligible, then the system will be balanced if the COG lies within the base of support. The COG measure does not account for the dynamic forces of faster motions and it has a limited ability to deal with external disturbances. As a result, only a few systems have been based on this measure. A more suitable measure that takes dynamics into account is called the center of pressure (COP). The COP is basically a weighted sum of vertical forces applied to the foot to find the location of the net applied force. Another way of describing the COP is the location where a single force vector could be applied without creating a moment about the foot, hence the zero moment point [18]. Fig. 3.23 compares the center of pressure with the center of gravity. For slow motions, the COP and COG coincide. The COP and COG remain within the base of support and thus the biped remains balanced. For fast motions, however, as the COM accelerates forward, the COP moves behind the COG. Then as the COM decelerates, the COP moves in front of the COM until it hits the edge of the foot and cannot move any further forward. The COM is still within the base of support, but the COP has moved to the boundary of support, indicating that foot rotation is about to begin and a fall is imminent. It should be noted that there is some debate in the literature about the equivalence of ZMP and COP, however, the differences are semantics. On a flat walking surface, it has been shown that the ZMP is mathematically equivalent to the COP [18], but according to Vukobratovic, COP and ZMP only coincide in a dynamically balanced gait. When the gait is not dynamically balanced, the ZMP does not exist. Lets now considered the elaboration done by Vukobratovic [39]. Walk is understood as moving “by putting forward each foot in turn, not having both feet off the ground at once.” From this definition, it transpires that walking is characterized by the displacement of legs such that both feet are not separated from the ground at the same time, which ensures that the body in the space (usually) moves forward. In view of the fact that the body is supported by the legs, ensuring that “the body in the space moves forward” is possible only if avoiding overturning is constantly taken care of, i.e. preserving the dynamic balance of

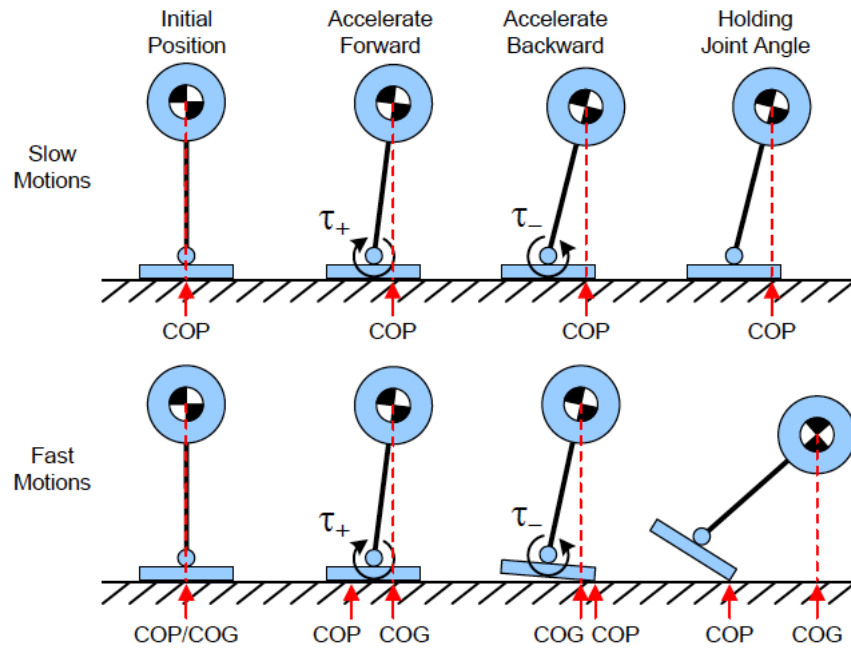


Figure 3.23. The use of center of gravity as a measure of balance is only acceptable when the motions are slow and the dynamic forces are negligible.

the mechanism.

Concept of ZMP related with locomotion

The characteristics of locomotions systems are:

- Unpowered DOF: contact foot-ground
- Gait repeatability (symmetry)
- Interchangeability of number of legs which are simultaneously in contact with the ground

As said in the above chapters during the walk there are two different situations in sequence:

- The statically stable double support phase
- The statically unstable single support phase

Thus the locomotion changes in structure during the walking cycle from an open to a closed kinematic chain (this is explained better in the following chapters). All of the joints are powered and directly controlled except for the ones formed by contact of the

foot and the ground. Thus the foot behavior can be controlled in an indirect way by ensuring appropriate dynamics, this means that the overall indicator of the mechanism's behavior is the ground reaction force in particular its intensity, direction and its action point (ZMP). Let's consider the single support phase: one foot is in contact with the ground while the other one is in the swing phase. To facilitate the analysis of a situation with moment and force like in Fig. 3.24 can be used, where the weight of the foot itself acts at its gravity center (point G). The foot also experiences the ground reaction at point P, whose action keeps the whole mechanism in equilibrium. To maintain the equilibrium

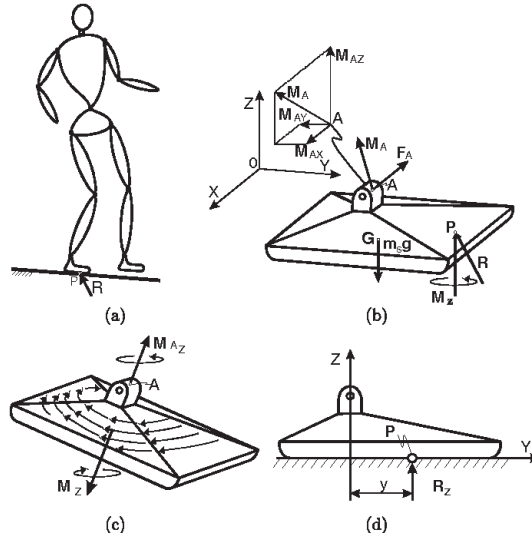


Figure 3.24. Support foot and influence of by the force, moment, ground reaction

the ground reaction force R should act at the appropriate point on the foot sole to balance all the forces acting on the mechanism during motion. The mechanism's position with respect to the environment depends on both the relative positions of the links and the relative position of the foot with respect to the ground. In order for the humanoid to perform the reference motion, it is necessary to realize the predefined motions at the joints, and at the same time preserve the relative position of the foot with respect to the ground. Therefore, to prevent the humanoid from falling, it is necessary to ensure the appropriate dynamics of the mechanism above the foot to preserve the regular contact of the supporting foot with the ground. In other words, since the sole-ground contact is unilateral, a necessary condition for avoiding overturning is that the motion of the humanoid as a whole is such that, while the regular sole-ground contact is preserved, the overall ground reaction can be replaced by one force only. If we introduce a Cartesian frame with the origin at the point where the resultant ground reaction (pressure) force is acting, with two axes (x and y) being tangential to the ground and the third (the z -axis) being normal, then a mathematical expression for the fulfillment of dynamic balance is: $\sum M_x = 0$ and $\sum M_y = 0$. The moments include gravity, inertial forces and other external forces acting on the humanoid body (like wind, different strike, etc.). It should

be noted that it is not necessary for the third component of the moment (about the z-axis) to be zero, provided it is compensated by the friction between the foot and ground. In such a case, $\sum Mz \neq 0$ does not influence the mechanism. The point inside the support area (excluding its edges) for which it holds that $\sum Mx = 0$ and $\sum My = 0$ is termed the Zero-Moment Point (ZMP). Thus the pressure under the supporting foot can be replaced by the appropriate reaction force acting at a certain point of the mechanism's foot. Since the sum of all moments of active forces with respect to this point is equal to zero it is named Zero Moment Point. The human dynamics will be modeled using the multi-body system consisting of N chains involving the body parts. Each chain consists of n_i -links interconnected with single DOF joints. During locomotion the following active motion forces act on the body links:

- G_i : gravitation force of the i-th link acting at the mass center C_i
- F_i : inertial force of the i-th link acting at the mass center C_i
- M_i : moment of the inertial force of the i-th link acting at the mass center C_i
- R: resultant ground reaction force

The first three are active motion forces and can be replaced by main resultant gravitational and inertial force and resultant inertial moment reduced at body CoM. The ground reaction force and moment can be decomposed into the vertical (moment of the friction reaction forces reduced at an arbitrary point P) and horizontal (friction force) components with respect to the reference frame. The foot-floor contact is assumed stable (without sliding), this means that the static friction forces compensate for the corresponding dynamic body reaction forces. Now, after this discussion, it can be considered again Fig. 3.24 and wrote mathematically what the equilibrium means:

$$R + F_A + m_S g = 0 \quad (3.1)$$

$$\vec{OP} \times R + \vec{OG} \times (m_S g) + M_A + M_z + \vec{OA} \times F_A = 0 \quad (3.2)$$

where:

- \vec{OP} radius vectors from the origin of the coordinate system O_{xyz} to the ground reaction force acting point (P)
- \vec{OG} radius vectors from the origin of the coordinate system O_{xyz} to the foot mass center
- \vec{OA} radius vectors from the origin of the coordinate system O_{xyz} to the ankle joint
- m_S is the foot mass.

If the origin of the coordinate system is placed at the point P and project Eq. 3.2 onto the z-axis, then the vertical component of the ground reaction moment (actually, it is the ground friction moment) will be:

$$M_z = M_{fr} = -(M_A^z + (\vec{OA} \times F_A)^z) \quad (3.3)$$

In a general case, this moment is different from zero and can be reduced to zero only by the appropriate dynamics of the overall mechanism. However, the projection of Eq. 3.2 onto the horizontal plane gives:

$$(\vec{OP}xR)^H + \vec{OG}x(m_Sg) + M_A^H + (\vec{OA}xF_A)^H = 0 \quad (3.4)$$

This equation is a basis for computing the position of the ground reaction force acting point (P). Eq. 3.4, representing the equation of the foot equilibrium, answers the above question concerning the ZMP position that will ensure dynamic equilibrium for the overall mechanism dynamics. In order to understand if for a given motion the mechanism is in dynamic equilibrium, the relationship between the computed position of P and the support polygon has been considered. If the position of point P, computed from Eq. 3.2, is within the support polygon, the system is in dynamic equilibrium. However, in reality, the point P cannot exist outside the support polygon, as in that case the reaction force R cannot act on the system at all. From this follows a conclusion: in reality, in order to ensure dynamic equilibrium, a point P that satisfies Eq. 3.2 must be within the support polygon. If the point P is outside the support polygon: in view of the fact that this position of P was obtained from the condition $M_x = M_y = 0$, we can consider it as a fictitious ZMP (FZMP). It is clear from Eqs. 3.4 and 3.1 that the ZMP position depends on the mechanism dynamics (i.e. on F_A and M_A). In the situation when the mechanism dynamics changes so that the ZMP approaches the support polygon edge (in either single-support or double-support phases) the corresponding point will remain the ZMP only if no additional moments are acting at this point. However, if an additional moment appeared, the locomotion mechanism would start to rotate about the foot edge and the mechanism would collapse. In such a situation, the acting point of ground reaction force would be on the foot edge. To further clarify the meaning of the ZMP outside the support polygon

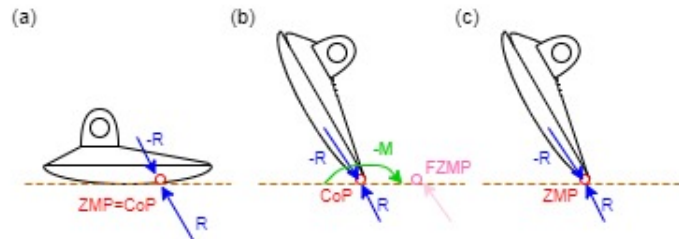


Figure 3.25. (a) dynamically balanced gait, (b) unbalanced gait where ZMP does not exist and the ground reaction force acting point is CoP while the point where $M_x = 0$ and $M_y = 0$ is outside the support polygon (FZMP). The system as a whole rotates about the foot edge and overturns, and (c) tip-toe dynamic balance

(FZMP) let reminded that there are two different cases in which the ZMP plays a key role:

- in determining the proper dynamics of the mechanism above the foot to ensure a desired ZMP position

- in determining the ZMP position for the given mechanism motion.

The second case is the one that is now elaborated because it refers to the gait control, where the ZMP position is a key indicator of the mechanism of dynamic equilibrium. ZMP position can be obtained by measuring forces acting at the contact of the ground and the mechanism, with the aid of force sensors on the mechanism's sole. If the biped gait is investigated using a dynamic model, the ZMP position must be computed. For a given mechanism motion, the force and moment at the ankle joint (F_A and M_A) can be obtained from the model of the mechanism dynamics, and all elements in Eq. 3.4 except for OP will be known. The procedure for determining ZMP position consists of two steps.

- Step 1. Compute OP from Eq. 3.4. Let's call the obtained position of the point P computed ZMP position.
- Step 2. The computed ZMP position is just a candidate to be a regular ZMP and its position should be compared with the real support polygon size. If the computed ZMP is outside the support polygon, this means that the ground reaction force acting point (P) is actually on the edge of the support polygon and the mechanism rotation about the support polygon edge will be initiated by the unbalanced moment, whose intensity depends on the distance from the support polygon edge to the computed position of ZMP, i.e. to the FZMP position.

In Step 1, it is obtained an answer to the question concerning the ZMP location for the given dynamics not taking into account the real foot size, whereas in Step 2, it is obtained the answer whether, regarding the foot size (more precisely, the support polygon size), the mechanism is really balanced or not, and where the regular ZMP (provided it exists) is located. If the computed acting point of the ground reaction force is within the real support polygon, this point is ZMP and the mechanism is in equilibrium. If this is not the case, the ground reaction force acting point will be on the support of the polygon border and the distance from it to the computed ZMP position is proportional to the intensity of the perturbation moment that acts on the foot.

In conclusion let us consider the single-support phase of a dynamically balanced gait of the mechanism having a one-link foot. The foot of the supporting leg is in contact with the support surface as presented in Fig. 3.26. Further, let us consider how to preserve dynamic balance of the mechanism and prevent it from falling. The answer is quite simple: by using an indicator that will warn of a critical situation approaching and it being necessary to undertake appropriate action to compensate. This indicator is the position of the ZMP inside the support area, and it corresponds to the position of the ground reaction force. The ZMP position inside the support area can easily be determined with the aid of force sensors on the sole, Fig. 3.27. All the time the ZMP is within the support area, there will be no rotation about the foot edge and the robot will preserve its dynamic balance. A warning means that the ZMP is coming closer to the foot edge [19]. Hence, the notion of the ZMP was introduced in order to control inertia forces. In the stable single support phase, the ZMP is equal to the COP on the sole. The advantage of the ZMP is that it is a point where the center of gravity is projected onto the ground in the static state and a

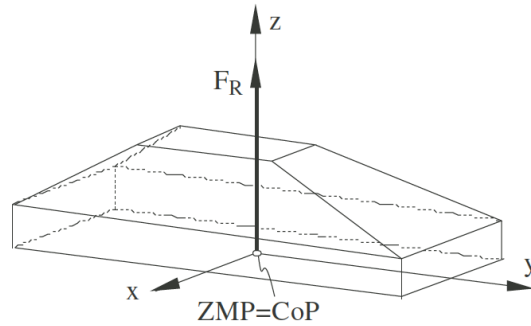


Figure 3.26. Foot of the supporting in the single-support phase

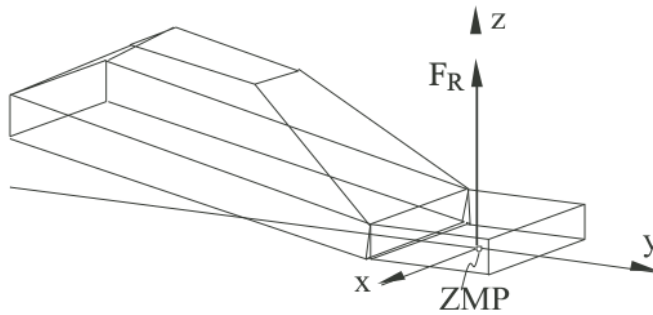


Figure 3.27. Rotation of the supporting foot about its edge.

point where the total inertial force composed of the gravitational force and inertial force of mass goes through the ground in the dynamic state. If the ZMP strictly exists within the supporting polygon made by the feet, the robot never falls down. Most research groups have used the ZMP as a walking stability criterion of dynamic biped walking. To this end, the robot is controlled such that the ZMP is maintained within the supporting polygon. In general, the walking control strategies using the ZMP can be divided into two approaches. First, the robot can be modeled by considering many point masses, the locations of the point masses and the mass moments of inertia of the linkages. The walking pattern is then calculated by solving ZMP dynamics derived from the robot model with a desired ZMP trajectory. During walking, sensory feedback is used to control the robot. Second, the robot is modeled by a simple mathematical model such as an inverted pendulum system, and then the walking pattern is designed based on the limited information of a simple model and experimental hand tuning. During walking, many kinds of online controllers are activated to compensate for the walking motion through the use of various sensory feedback data including the ZMP. The first approach can derive a precise walking

pattern that satisfies the desired ZMP trajectory, but it is hard to generate the walking pattern in real-time due to the large calculation burden. Further, if the mathematical model is different from a real robot, the performance is diminished. On the contrary, the second approach can easily generate the walking pattern online. However, many kinds of online controllers are needed to compensate for the walking pattern in real-time, because the prescribed walking pattern cannot satisfy the desired ZMP trajectory. In addition, this methods depends strongly on the sensory feedback, and hence the walking ability is limited to the sensor's performance and requires considerable experimental hand tuning [8].

3.6 Model for biped robots

This section is partially done in collaboration with Congedo Gabriele [2].

3.6.1 Linear Inverted Pendulum Model (LIPM)

Linear inverted pendulum model (LIPM) Fig. 3.28 is an effective and widely used simplified model for biped robots.

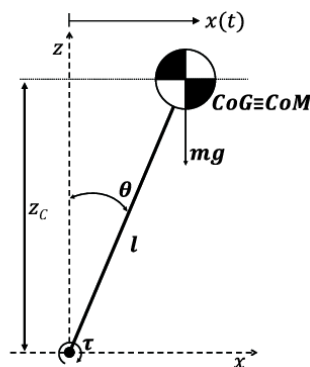


Figure 3.28. Linear Inverted Pendulum Model

However, LIPM includes only the single support phase (SSP) and ignores the double support phase (DSP). In this situation, the acceleration of the center of mass (CoM) is discontinuous at the moment of leg exchange, leading to a negative impact on walking stability. If the DSP is added to the walking cycle, the acceleration of the CoM will be smoother and the walking stability of the biped will be improved. Compared with other types of robots, humanoid robots have good adaptability to the environment, stronger obstacle avoidance ability, and a smaller moving blind area, which has attracted the attention and in-depth research of scholars. At present, biped robots are still quite far away from the real sense of anthropomorphism, and there are many problems to be solved in this field. For example, due to the inherent instability of biped walking, walking stability analysis is still an important issue for biped robots. In addition, the biped robot is a

high-order and strong coupling nonlinear system, which makes the trajectory planning and control difficult. The realization of stable walking is the primary task in the research of humanoid robots. There are many methods for gait planning of biped robots. These methods could be divided into two classes. The first uses the accurate information of dynamical parameters to generate walking patterns. Joint angle trajectories or trajectories of some key parts, e.g. hip and/or feet, are usually fitted by spline or polynomial functions, then the coefficients of spline or polynomial functions are determined by parameter optimization technique. However, these gait-planning methods need a lot of computation and cannot meet the requirement of trajectory planning in real time. The more degrees of freedom and the higher the order of the polynomials, the more computation time is needed for solving the optimization problem. The other class is based on a simplified model to generate walking patterns. Inverted pendulum is widely used because of its simplicity. A biped robot is usually regarded as a concentrated mass and massless leg. The trajectory of the center of mass (CoM) is planned with a simplified model, and then the angles of other joints are solved by inverse kinematics. One of the widely used methods is the linear inverted pendulum model (LIPM). The advantage of LIPM is that the trajectory of the CoM has an analytical solution. Moreover, its forward and lateral motions are decoupled. Another model is the inverted pendulum model (IPM) with constant leg length. In this model, the CoM moves along an arc. Although the dynamic equation of IPM is simple, there is no analytical solution due to its nonlinearity. The disadvantages of LIPM and IPM are that they can only generate the trajectory of the single support phase (SSP), but cannot generate the trajectory of the double support phase (DSP). From an application perspective, when the biped robot is walking outdoors, due to the unstructured ground environment, the robot is required to have the ability of real-time gait generation according to the current environment. However, the more accurate the model is, the more computation is needed. Hence real-time gait planning may become very difficult. Therefore, the simplified model is a feasible and very useful method for real-time gait planning. On the other hand, there is little attention on the DSP. Many gait planning methods consider only the SSP and ignore the DSP, or the DSP is assumed to be instantaneous. In this situation, the center of pressure (CoP) or zero-moment point (ZMP) needs to transfer from the trailing foot to the leading foot instantaneously when the support leg is switched. This requires an impulsive force between the rear foot and the ground. The emerge of impulsive force could lead to some adverse factors:

- it has a negative effect on the walking stability analysis;
- generating impulse force needs a sufficiently large joint torque that the joint driving motors may not provide;
- it may damage the hardware of the robot.

The introduction of the DSP can reduce the impact between the foot and the ground, make a smooth ZMP transition from the trailing foot to the leading foot, and improve walking stability. In addition, the support polygon area of the DSP is larger than that of the SSP, so the ground can provide greater external torque to the robot during the DSP. Therefore, the robot has stronger state-adjustment ability during the DSP. During the SSP, because

the robot's foot is small, the ground cannot provide a large enough external torque to avoid the robot falling down; as a result, the robot needs more adjustment of the internal state. Kajita and Tani reported that adding the DSP to the LIPM reduced the loss of the CoM's velocity when the support leg exchanges [20]. To overcome shortcomings of models without the DSP, some scholars introduced the DSP in gait planning. [21] planned the CoM's trajectory of the DSP as a fourth order polynomial function. The coefficients of the polynomial are determined by the boundary condition and the specified duration of the DSP. [22] design the CoM's trajectory in the DSP as a fifth order polynomial function. The disadvantage of their method is that walking stability was not taken into consideration during the DSP. With the increase of the order of the polynomial, unexpected oscillation of CoM may occur; as a result, unexpected the CoM during the DSP is not intuitive and cannot be perfectly integrated with LIPM. [23] propose the linear pendulum model (LPM) to plan the trajectory of the CoM in the DSP, and determine the appropriate suspension point, which can ensure that the acceleration of the CoM is continuous at the moment of the switch between the SSP and the DSP. However, they only plan the cyclic gait of the robot on the horizontal ground, and do not give the gait-planning method when the robot faces a more complex environment. [24] extends the results of [23] to generate DSP trajectories in two situations. One is to land the swing leg earlier than planned, and the other is trajectory planning to stop walking in the DSP. However, they still did not put forward the method in more situations. In this work, LIPM and LPM are used to plan the trajectories of the SSP and the DSP, respectively. The dynamic equations of LIPM and LPM are linear, so they have analytic solutions. Trajectory planning only needs a small amount of computation. Through dynamic analysis of two pendulum models and their ZMP, the stability of gait can be guaranteed. Moreover, LPM is well-compatible with LIPM.

3.6.2 3D Linear Inverted Pendulum Model (3D-LIPM)

The 3D-LIPM is a point mass and a massless rod. Let's define:

- $p=(x,y,z)$: position of the mass
- r : length of the rod
- θ_p : angle of the rod wrt x
- θ_r angle of the rod wrt y

The pendulum position equations are:

$$x = r \sin(\theta_p) \quad (3.5)$$

$$y = -r \sin(\theta_r) \quad (3.6)$$

$$z = r \sqrt{(1 - \sin(\theta_r)^2 - \sin(\theta_p)^2)} \quad (3.7)$$

While the motion equation is:

$$\begin{pmatrix} \tau_r \\ \tau_p \\ f \end{pmatrix} = m \begin{pmatrix} 0 & -rc(\theta_r) & -\frac{rc(\theta_r)s(\theta_r)}{\sqrt{(1-s(\theta_r)^2-s(\theta_p)^2)}} \\ rc(\theta_p) & 0 & -\frac{rc(\theta_p)s(\theta_p)}{\sqrt{(1-s(\theta_r)^2-s(\theta_p)^2)}} \\ s(\theta_p) & -s(\theta_r) & -\sqrt{(1-s(\theta_r)^2-s(\theta_p)^2)} \end{pmatrix} + mg \begin{pmatrix} -\frac{rc(\theta_r)s(\theta_r)}{\sqrt{(1-s(\theta_r)^2-s(\theta_p)^2)}} \\ -\frac{rc(\theta_p)s(\theta_p)}{\sqrt{(1-s(\theta_r)^2-s(\theta_p)^2)}} \\ -\sqrt{(1-s(\theta_r)^2-s(\theta_p)^2)} \end{pmatrix}$$

The dynamic along x is:

$$m(z\ddot{x} - x\ddot{z}) = \frac{\sqrt{(1-s(\theta_r)^2-s(\theta_p)^2)}}{c(\theta_p)}\tau_p + mgx \quad (3.8)$$

The dynamic along y is:

$$m(-z\ddot{y} + y\ddot{z}) = \frac{\sqrt{(1-s(\theta_r)^2-s(\theta_p)^2)}}{c(\theta_r)}\tau_r + mgy \quad (3.9)$$

The pendulum motion can be constrained in the xy, considering that the oscillations around the z are small compared to the others. The constrain plane is represented by the respective normal vector $(k_x, k_y, -1)$ and by its z intersection z_c [26]:

$$z = k_x x + k_y y + z_c \quad (3.10)$$

Replacing 3.10 and its second derivative in 3.8 and 3.9:

$$\ddot{x} = \frac{g}{z_c}x + \frac{k_y}{z_c}(x\ddot{y} - \ddot{x}y) + \frac{1}{mz_c} \frac{\sqrt{(1-s(\theta_r)^2-s(\theta_p)^2)}}{c(\theta_p)}\tau_p \quad (3.11)$$

$$\ddot{y} = \frac{g}{z_c}y - \frac{k_x}{z_c}(x\ddot{y} - \ddot{x}y) - \frac{1}{mz_c} \frac{\sqrt{(1-s(\theta_r)^2-s(\theta_p)^2)}}{c(\theta_r)}\tau_r \quad (3.12)$$

If the plane is flat $k_x = k_y = 0$:

$$\ddot{x} = \frac{g}{z_c}x + \frac{1}{mz_c} \frac{\sqrt{(1-s(\theta_r)^2-s(\theta_p)^2)}}{c(\theta_p)}\tau_p \quad (3.13)$$

$$\ddot{y} = \frac{g}{z_c}y - \frac{1}{mz_c} \frac{\sqrt{(1-s(\theta_r)^2-s(\theta_p)^2)}}{c(\theta_r)}\tau_r \quad (3.14)$$

If small oscillations around x and y are considered:

$$\ddot{x} = \frac{g}{z_c}x + \frac{1}{mz_c}\tau_p \quad (3.15)$$

$$\ddot{y} = \frac{g}{z_c}y - \frac{1}{mz_c}\tau_r \quad (3.16)$$

These are linear equations, if the plane is not flat an additional constrain can be added:

$$\tau_x x + \tau_y y = 0 \quad (3.17)$$

This means that the plane inclination does not affect the horizontal motion. For the 3D-LIMP constrained horizontally ($k_x = k_y = 0$), the ZMP position on the floor (p_x, p_y) can be easily calculated:

$$p_x = -\frac{\tau_p}{mg} \quad (3.18)$$

$$p_y = \frac{\tau_r}{mg} \quad (3.19)$$

Substituting 3.18 and 3.19 in 3.15 and 3.16:

$$\ddot{x} = \frac{g}{z_c}(x + p_x) \quad (3.20)$$

$$\ddot{y} = \frac{g}{z_c}(y - p_y) \quad (3.21)$$

3.6.3 The cart-table model

This subsection describes the study done by [1].

To control the ZMP it has to be the output of the systems. In the previous section we have described the relationship that exists between the ZMP position and the 3D-LIMP model in 3.20 and 3.21. Rewriting them to have the ZMP as their output we obtain:

$$p_x = x - \frac{z_c}{g}\ddot{x} \quad (3.22)$$

$$p_y = y - \frac{z_c}{g}\ddot{y} \quad (3.23)$$

A model that directly corresponds to these equations is the cart-table model. It consists in a running cart of mass m on a pedestal table whose mass is negligible. The foot of the table is too small to let the cart stay on the edge. However, if the cart accelerates at a proper rate, the table can keep upright for a while. At this moment, the ZMP exists inside the table foot. The ZMP moments must be zero, thus the torque around the axis x will be:

$$\tau_{zmp} = mg(x - p_x) - m\ddot{x}z_c = 0 \quad (3.24)$$

In the same way can be found the ZMP torque equation for the y -axis. The motions on x and y are uncoupled, and planar motion occurs at z_c . If the ZMP control is taken into account as a servo control problem, it is possible to put 3.22 in the form of a state variable, including the time derivative of the acceleration as input as shown by:

$$\frac{d}{dt} \begin{pmatrix} x \\ \dot{x} \\ \ddot{x} \end{pmatrix} = \begin{pmatrix} 0 & 1 & 0 \\ 0 & 0 & 1 \\ 0 & 0 & 0 \end{pmatrix} \begin{pmatrix} x \\ \dot{x} \\ \ddot{x} \end{pmatrix} + \begin{pmatrix} 0 \\ 0 \\ 1 \end{pmatrix} u_x \quad (3.25)$$

$$p_x = \begin{pmatrix} 1 & 0 & \frac{z_c}{g} \end{pmatrix} \begin{pmatrix} x \\ \dot{x} \\ \ddot{x} \end{pmatrix} \quad (3.26)$$

Katayama et al. [27] have proposed the optimal preview servo controller technique to obtain the CoG pattern which tracks the ZMP reference. First the system in the equations 3.25 and 3.26 must be discretized with sampling time of ts as:

$$x(k+1) = Ax(k) + Bu(k) \quad (3.27)$$

$$p(k) = Cx(k) \quad (3.28)$$

where:

$$x(k) = \begin{pmatrix} x(kT) & \dot{x}(kT) & \ddot{x}(kT) \end{pmatrix}^T \quad (3.29)$$

$$u(k) = u_x(kT) \quad (3.30)$$

$$p(k) = p_x(kT) \quad (3.31)$$

$$A = \begin{pmatrix} 1 & T & \frac{T^2}{2} \\ 0 & 1 & T \\ 0 & 0 & 1 \end{pmatrix} \quad (3.32)$$

$$C = \begin{pmatrix} 1 & 0 & -\frac{z_c}{g} \end{pmatrix} \quad (3.33)$$

In this way is obtained the state-space representation of the dynamics of the cart-table model. With the given reference of ZMP $p^{ref}(k)$, the performance index is specified as:

$$J = \sum_{i=k}^n (Q_e e(i)^2 + \Delta x^T Q_x \Delta(i) + R \Delta u^2) \quad (3.34)$$

where:

$e(i) = p(i) - p^r f(i)$ is a servo error

$Q_e, R > 0, Q_x$ is a symmetric non-negative definitive matrix

$\Delta x(k) = x(k) - x(k-1)$ is the incremental state vector

$\Delta u(k) = u(k) - u(k-1)$ is the incremental input

When the ZMP reference can be previewed for N_L step future, at every sampling time, the optimal controller proposed by Kajita et al. which minimizes the performance index 3.35 is:

$$u(k) = -G_i \sum_{i=0}^k e(i) - G_x x(k) - \sum_{j=1}^{N_L} G_p(j) p^{ref}(k+j) \quad (3.35)$$

The gains G_i, G_x and $G_p(j)$ are calculated from the weights Q_e, Q_x and R and the systems parameter of 3.27 and 3.28. The problem solved by Kajita et al. [26] is a discrete-time,

infinite-horizon LQR problem. This method required high computation, but generalized the specification as the optimization of a quadratic cost which could balance ZMP tracking against CoM acceleration, giving a more robust CoM output. Three terms are included in the preview controls (3.35): the integral action on the tracking error, the state feedback and the preview action on the future reference.

3.6.4 The Spherical Inverted Pendulum

In this subsection it is explained the concepts described by [40], [41] and [42].

In the first paper [40] the Foot Placement Estimation (FPE) method has recently been extended to 3-D spaces by adopting a specific form of a spherical inverted pendulum (SIP). The approach doesn't involve dynamics, but it is based solely on energies and momenta, however the authors (DeHart et al.) introduced several approximations, in order to reach a manageable solution. The scope of the study is to revisit the spherical inverted pendulum applied to walking biped, offering an exact solution to the gait and the FPE by using symbolic computation. This is facilitated by exploiting Kane's approach to dynamical modeling, and his software environment for symbolic manipulation, called Autolev. It generates explicit formulas describing the energies and angular momenta before/after the impact, along with the mechanics of the impact. As the resulting equations, function of (measurable) angular positions and velocities, are very compact, embedded in a numerical nonlinear solver, are suitable to be implemented in real-time and used in practice to control biped robots or lower limb exoskeletons. The walk with the SIP, based on energy, has been compared to the simulation of a 12 degrees of freedom biped robot tracking preview signals using the Zero Moment Point (ZMP) of the Linear Inverted Pendulum (LIPM). This quantitatively shows the inefficiency, in terms of energy, of the ZMP based walk, and the gain due to the recovery of the collision of the flying foot.

In the second paper [41] the walk design is approached by a 3-D inverted pendulum in a polar coordinate system. The advantage of this model is to easily offer indications of the energy expenditure of an efficient walk. However, the disadvantages that were never recognized by authors previously using this model is that the COG trajectory has to pass through the supporting foot location. This causes an unnecessary and unrealistic waving in the frontal plane during gait. The problem is solved by extending the model of the inverted pendulum by introducing the pelvis width and the distance between the hips of the two legs, without adding dynamical complexity.

In the third paper [42] the classical walk in biped robotics was obtained by controlling balance during the whole step, i.e. guaranteeing that the pressure point under the soles always stayed in the polygon of the supporting feet. However, this assumed that the feet were able to transfer torque to the ground during the whole gait cycle, in spite of the fact that the amount of transferable torque in the feet-ground contact is limited, it is possible only during some phases of the step, and finally the overall process is energetically inefficient. On the other hand, starting from the passive motion of the rimless wheel falling on an inclined surface, and ending to the inverted pendulum with a compass, stability

in the whole was proven in spite of dynamical instability inside each step. Along this line results of Foot Placement Estimation (FPE) in 2-D and 3-D showed how an energy efficient walk was possible, emulating the human walk with a free fall on the swing foot and energy restitution at the foot collision with the ground for the next step. This model assumes pointy feet, so without torque transfer to the ground. In previous papers, in the realm of FPE, adopted the 3-D inverted pendulum in polar coordinates (Spherical Inverted Pendulum - SIP) to introduce omnidirectional walks with arbitrarily changing characteristics. No torque control was used during the step, i.e the pendulum was always in free fall, the only control actions were at the beginning of the next step. These actions are: the change of angular velocities at the start of a new step, and the preparation of the position in the frontal and sagittal planes of the swing foot for the next collision. The [42] concludes this novel paradigm, proposing the most general model to account for all characteristics of the biped and of the gait, with adding a minimum of dynamical complexity. This model allows, not only to walk on a flat surface, but also to go up and down stairs.

3.6.5 Final Considerations

The LIMP model is a good approximation of the humanoid robot motion dynamics which results in a natural motion of the CoG, but has not a direct link with the position of the ZMP on the ground. It is true that the acceleration of the CoG is strictly related to its position and to that of the ZMP, as reported by 3.20 and 3.21, but the inverse equations that compute the position of the ZMP from the acceleration and position of CoG corresponds to a different model, the cart-table. Furthermore, there is a discontinuity during the double support phase, when changing stance leg. The jerk (the time derivative of the acceleration) is not taken into account, thus there is low performance at high speeds, when it influences the biped dynamics. From the cart-model it is possible to derive a controller for the ZMP preview like the 3.35. The preview control can also optimize the jerk, and the cart-table is continuous all the time, no matter the gait phase. For these reasons the cart-table model is usually preferred for the development of a controller. There are other approaches for solving the cart-table problem, like the solution proposed by Choi et al [3]. The discrete-time LQR problem proposed by Kajita [25][26] has been of great impact: its bigger contribution in biped control theory is that he has developed a method that takes into account the ZMP preview as well the quality of the CoM motion dynamics. From its method, other approaches for optimizing controllers of the ZMP preview are derived, such as Russ Tedrake et al. [4] optimal ZMP tracking controller, which solves the continuous-time LQR problem in an iterative manner without taking into account the jerk. This approach is used in this thesis for the CoM trajectory generation. [1]

Chapter 4

Instrumentation

This section is entirely done in collaboration with Congedo Gabriele [2].

From the study of [1], in gait analysis the biomechanics of human motion, can be evaluated with different methods and instrumentation. These methods can be classified according to various criteria. For example they can be categorized into non-wearable or wearable sensors:

- Non-wearable sensors are those that cannot be placed on a specific part of the body. However, they interact with the patient through their contacts. Some examples in this category are force plates and instrumented treadmills.
- Wearable sensors, of several types, with different measurement accuracy and purposes. It can be found in markers, accelerometers, gyroscopes, magnetometers, electrodes for EMG and many others.

4.1 Non-wearable sensors

4.1.1 Force transducers and force plates

To measure the force exerted by the human body on an external body or load suitable force-measuring devices are needed. Such a device, called force transducer, generates an electrical signal proportional to the applied force. There are many kinds available: strain gauge, piezoelectric, piezoresistive, capacitive, and others. All these work on the principle that the applied force causes a specific strain within the transducer [28]. In particular:

- For the gauge type, a calibrated metal plate or beam within the transducer undergoes a tiny change (strain) in one of its dimensions.
- Piezoelectric requires slight deformations of the atomic structure within a block of special crystalline material, such as quartz. Deformation of its crystalline structure changes the electrical characteristics such that the electrical charge across appropriate surfaces of the block is altered and can be translated via suitable electronics to a signal proportional to the applied force.

- Piezoresistive types exhibit a change in resistance which, like the strain gauge, upset the balance of a bridge circuit.

4.1.2 Treadmills

Recently it is becoming more popular to use treadmills for gait studies. They can be combined with cameras, marker systems, and force platforms can be inserted directly under the rollers. The use of treadmills in gait analysis has made it possible to record straight line walking that can go beyond the distance covered in a laboratory limited by the cameras. It's also much easier to set a walking speed and it's also possible to conduct experiments with different inclinations w.r.t. the ground. However, depending on the future use of the recorded data, one of the disadvantages may be that the space-temporal recordings of the markers remain confined in the treadmill dimensions instead of advancing meter by meter like a real walk, so this data may need further adjustments [29].

4.2 Wearable sensors

4.2.1 Optoelectronic stereophotogrammetry

It's a technique that involves cameras to capture the trajectory of spherical retroreflective markers attached to the desired locations of the body. With stereophotogrammetry can be evaluated, with a good precision, movement and orientation of each body segment. It enables realistic reconstructions and representations of the musculoskeletal system during a certain motion task. For these reasons it is considered one of the best instrumentation for gait analysis [30]. By the way, it also suffers a bit from trajectory gaps, it takes long time for preparation and the space for analysis is restricted to the area in which the cameras are operating. In addition, it is expensive.

4.2.2 Accelerometer

It's a measurement device whose output consists of the proper acceleration, the acceleration of the body on which is attached w.r.t. its instantaneous coordinate frame. Accelerometers can be single or multi-axis and detect magnitude and direction of the acceleration, seen as a vector quantity. In most accelerometers, the physical principle exploited to measure the acceleration is based on the inertia of a mass subjected to an acceleration. An elastic element suspends a mass, and this mass, in case of acceleration, moves from its rest position. Equating Hooke's law to Newton's law is obtained $kx = ma$ and it can be seen that the displacement of the elastic element is proportional to the mass acceleration. A displacement-sensitive sensor transforms it into an electrical signal [30]. There are many types of accelerometers, such as capacitive, strain gauge, piezoresistive and piezoelectric. For gait analysis the most commonly used are capacitive and piezoresistive.

4.2.3 Gyroscope

They measure the angular velocity around their sensing axis. Typically they are mechanical and consist of a rotating device which maintains fixed its rotating axis exploiting the conservation of angular momentum law. A 3D gyroscope can be described as a wheel mounted in three gimbals, which are the pivoted supports that enable the rotation around three different axes. The fundamental equation describing a rotating rigid system is the following one.

$$M = \frac{dL}{dt} = \frac{d(I\omega)}{dt} \quad (4.1)$$

Where M is the torque, L the momentum, I the inertia and ω the angular velocity. The derived motion is the precession, and the reaction force induces the gyroscope to rotate around a fixed axis, called spin axis, which does not change its direction even if the support varies its orientation. Thanks to the development of MEMS, miniaturized gyroscopes can become widespread. They consist of a vibrating element that, if subjected to a rotation, is also affected by a vibration in the orthogonal direction to the original one, according to the Coriolis effect [30]:

$$F = -2m(\omega \times v) \quad (4.2)$$

F is the Coriolis force, ω the angular velocity and v the linear velocity of the mass m .

4.2.4 Magnetometer

A magnetometer is a measuring device that detects a magnetic field. A scalar magnetometers measure the magnitude of the magnetic field directly, while the vectorial ones measure the direction and the strength of the magnetic field detecting the component along a particular axis. Using a three axial magnetometer, thus knowing the components of the magnetic field in three different and independent directions, allows to determine the vector in 3D space [30].

$$h = (h_{earth} + h_{external})n \quad (4.3)$$

The above equation represents a single axis magnetometer model, where n is the sensing axes. The most common of the magnetometers is the compass, which points in the direction of the Earth's magnetic north.

4.2.5 Inertial Measurement Units

In many fields, such as navigation, robotics and motion analysis, it is needed to know as precisely as possible the angular position in the space of objects. So for an accurate estimation of the orientation of a rigid body, w.r.t. an inertial frame, an Inertial Measurement Units (IMU) can be used. They are composed of two sensors, a gyroscope which measures the angular rate, and an accelerometer which measures the linear and gravity acceleration. With these two sensors an IMU can estimate its attitude. But since the accelerometer is not sensitive to the rotation around the gravity axis, an additional reference vector is needed to estimate the heading direction. Recent studies have discovered that combining

an accelerometer with a magnetometer makes it possible to find out both attitude and heading directions. This system is called Magneto-Inertial Measurement Units or MIMU [30]).

4.2.6 Electrogoniometers

An electrogoniometer is an electronic device that uses angle sensors, such as potentiometers, strain gauges and, more recently, accelerometers, appropriately positioned across a joint to measure its angle. It gives good results when used for body movements where we have limited speed and amplitude [31]. The most common electrogoniometers employ one of the following three sensor schemes:

- In Potentiometric Electrogoniometer an electrical resistance can be used to determine the angle between the joints. These types of electrogoniometers are somewhat bulky and restrict patient movement.
- For the Flexible Electrogoniometer the strain gauge mechanism is housed inside a spring, which changes its electrical resistance proportionally to the variation of the angle between the plastic end blocks longitudinal axes.
- Optoelectronic Systems are video systems that use one or more video cameras to track bright markers placed at various locations on the patient's body. The system keeps track of the vertical and horizontal coordinates of each marker, and a software processes this information to determine the angle on the body segments of interest.

4.2.7 Optical fiber sensors

These sensors are made of flexible plastic optical fibers (OFS) through which optical signals are transmitted. The basic components of an OFS-based system are a light source, a flexible optical fiber and a photodetector. The light source at one of the extremities generates the optical signal, which travels through the flexible optical fiber and is received by the photodetector at the other extremity of the fiber. By measuring the attenuation of the optical signal, it is possible to determine the bending angle of the fiber. Due to this simple sensing principle and structure, OFS can be easily integrated into a monitoring system for measuring human joint angles. The main benefits of OFS are high resolution, flexibility, light-weight and immunity to electromagnetic interference [32].

4.2.8 Textile-based sensors

Textile-based sensors are very suitable for developing a wearable joint monitoring system. The working principles of all these sensors are similar. In all cases, changes of resistance are measured, and these changes are directly related to the corresponding joint angles. To develop a long-term and regular wearable monitoring device, textile-based sensors can be a good choice because of their flexibility and simple sensing principle. Furthermore, they can be easily integrated into stretchable skin-tight fabrics around the joints. The measurement parameter is the resistivity change of the conductive wire w.r.t. the joints movement [32].

4.2.9 EMG signals

The electrical signal associated with the contraction of a muscle is called an electromyogram, or EMG. The study of EMGs is called electromyography. An EMG signal increases in amplitude as the intensity of the voluntary muscle activity it quantifies increases. Electrodes are used for their recording and can be divided into two main groups, surface and indwelling electrodes. For both groups, the basic function is linked to the correct positioning on the patient (position and surface of contact) and the appropriate adjustment of the amplifier with which they operate (Instrumentation Amplifier). EMG signals, depending on the application and specifications of the acquisition system, once recorded are processed with, for example, filters and rectifiers. EMG signals are a fundamental tool in the analysis of muscle behavior associated with a particular task: for this reason they are widely used in gait analysis [12].

Chapter 5

Biped design

The biped design was initially created using SketchUp (3D design software), subsequently it was created using Onshape (CAD software system).

5.1 SketchUp

SketchUp was chosen as 3D design software because it is a very simple tool and it allows me to quickly create the desired design.

It is a computer graphics application for 3D modeling, originally created by Last (founded in 2000 by Brad Schell and Joe Esch) and oriented towards architectural design, urban planning, civil engineering, video game development and related professions [33].

With this software each component is created to safely support a patient undergoing rehabilitation.

The measures of the structure are:

- Height: 1579mm
- Width: 473mm
- Thickness is not always the same, it varies between 10mm and 43mm

The figures 5.1 show the entire structure of the biped.

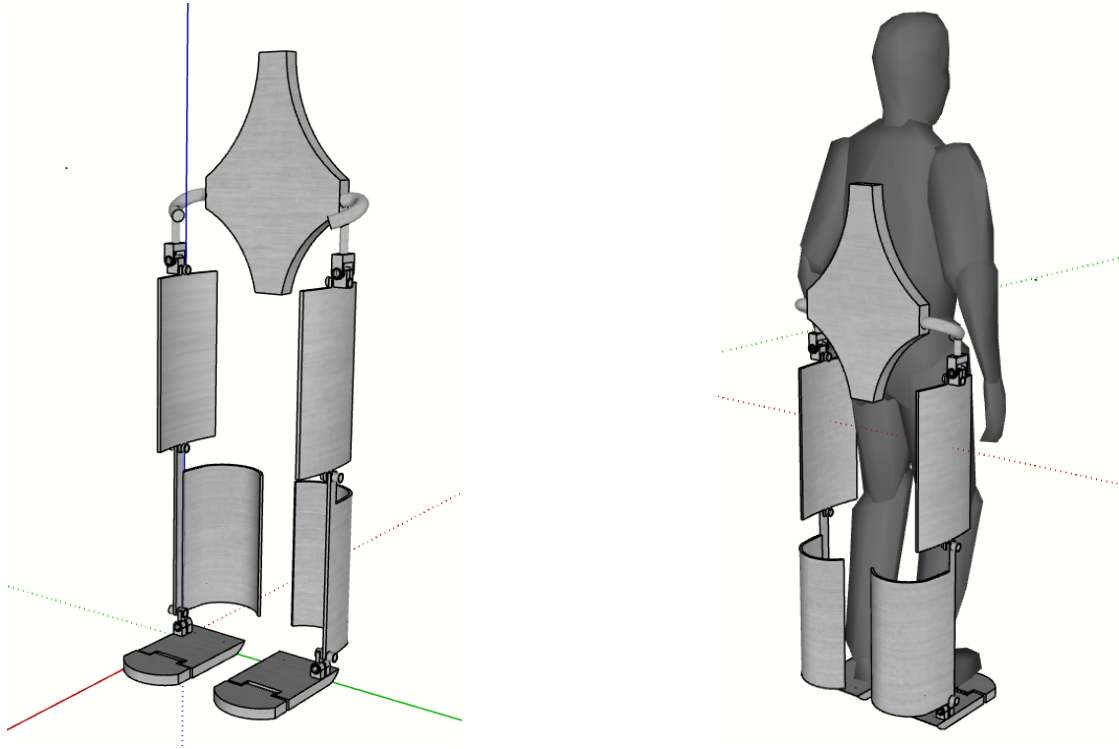


Figure 5.1. Biped design on SketchUp

5.2 Onshape

Onshape was chosen in order to implement everything on Matlab.

Onshape is a computer-aided design (CAD) software system, delivered over the Internet via a Software as a Service (SAAS) model.

It makes extensive use of cloud computing, with compute-intensive processing and rendering performed on Internet-based servers, and users are able to interact with the system via a web browser or the iOS and Android apps [33].

In the 5.2 is shown the prototype. In this structure the arrows shown in the image represent the degrees of freedom for each joint, in total there are 6-Dof for each leg.

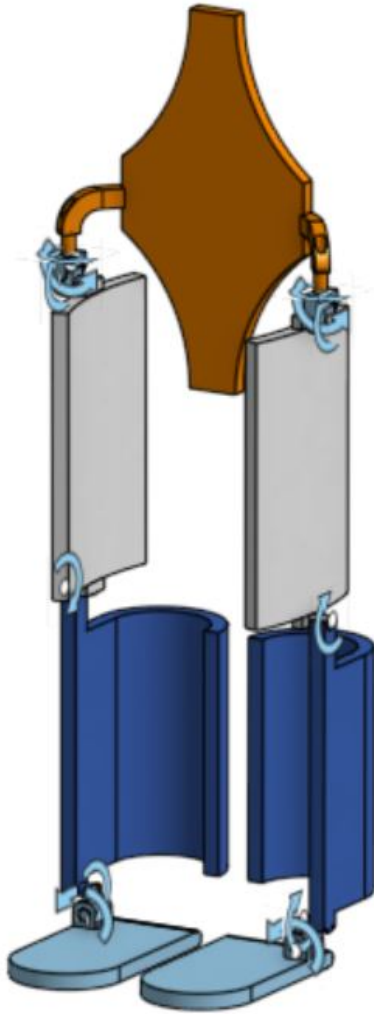


Figure 5.2. Prototype created on Onshape

This model was imported on Matlab in order to see the kinematic chain on Simulink, it can be seen in Fig. 5.3.

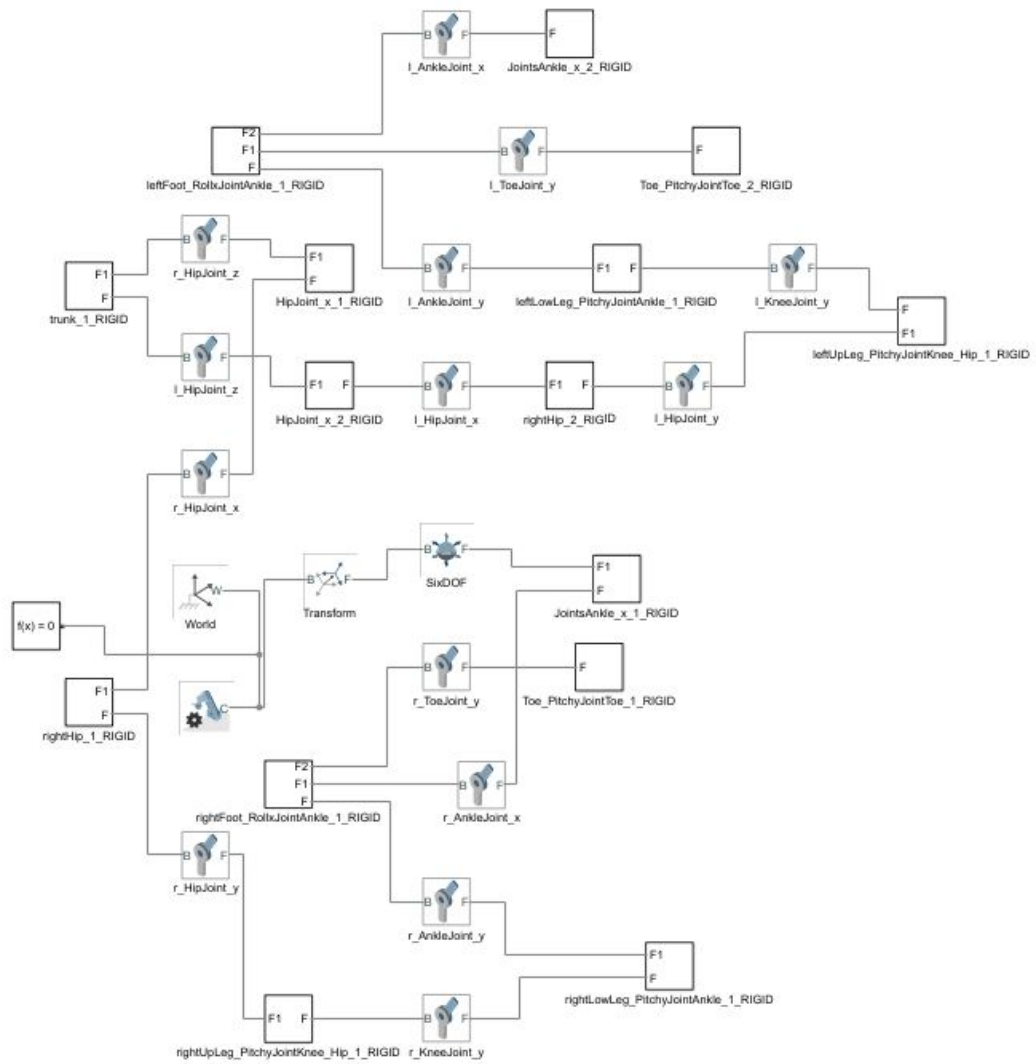


Figure 5.3. Kinematic chain on Simulink

Chapter 6

Theoretical study of kinematics

In this chapter there are references to [7] and [34]. As is shown in 6.1 in this study is considered a 14 degrees of freedom (Dof) biped: 3 Dof for the waist, 1 Dof for the knee, 2 Dof for the ankle and 1 Dof for the toe. Each leg can be modeled as a kinematic chain with eight links connected by seven revolute joints.

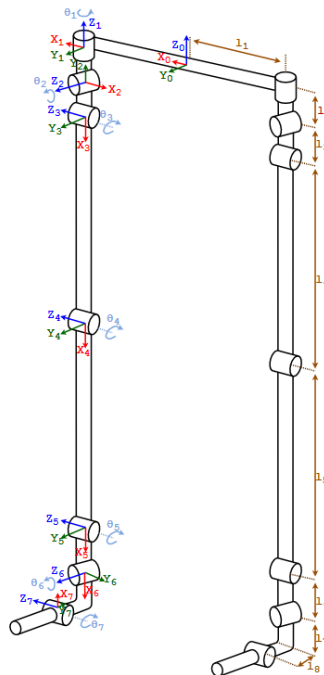


Figure 6.1. Kinematic description of the robot legs

6.1 Forward Kinematics

In order to calculate the end effector (toe) position is used the DH convention: first the following table has been created,

DH parameters	Joint 1	Joint 2	Joint 3	Joint 4	Joint 5	Joint 6	Joint 7
θ_i	θ_1	θ_2	θ_3	θ_4	θ_5	θ_6	θ_7
d_i	0	$-l_2$	0	0	0	0	l_8
a_i	l_1	0	l_3	l_4	l_5	l_6	$-l_7$
α_i	0	$\pi/2$	$\pi/2$	0	0	$-\pi/2$	$-\pi/2$

then with the following transformation matrix i relate the i-th coordinate frame to the (i-1)th coordinate frame,

$$A_i = \begin{bmatrix} C_{\theta_i} & -S_{\theta_i}C_{\alpha_i} & S_{\theta_i}S_{\alpha_i} & a_iC_{\theta_i} \\ S_{\theta_i} & C_{\theta_i}C_{\alpha_i} & -C_{\theta_i}S_{\alpha_i} & a_iS_{\theta_i} \\ 0 & S_{\alpha_i} & C_{\alpha_i} & d_i \\ 0 & 0 & 0 & 1 \end{bmatrix}$$

at the end using the following product between all the matrices $T_7^0 = A_1^0 A_2^1 A_3^2 A_4^3 A_5^4 A_6^5 A_7^6$ the toe position vector results in:

$$p_x = l_1 C_1 + l_3 C_{12} C_3 + l_4 (S_4 S_{12} + C_3 C_4 C_{12}) + l_5 (S_{12} S_{45} + C_{12} C_3 C_{45}) + l_6 (S_{12} S_{456} + C_{12} C_3 C_{456}) + l_7 (-S_{12} C_7 S_{456} - C_7 C_{12} C_3 C_{456} + S_3 S_7 C_{12}) + l_8 (S_{12} C_{456} - C_{12} C_3 S_{456})$$

$$p_y = l_1 S_1 + l_3 C_3 S_{12} + l_4 (-S_4 C_{12} + C_3 C_4 S_{12}) - l_5 (C_{12} S_{45} - S_{12} C_3 C_{45}) - l_6 (C_{12} S_{456} - S_{12} C_3 C_{456}) + l_7 (C_7 C_{12} S_{456} - C_7 S_{12} C_3 C_{456} + S_3 S_7 S_{12}) - l_8 (C_{12} C_{456} + S_{12} C_3 S_{456})$$

$$p_z = -l_2 + l_3 S_3 + l_4 C_4 S_3 + l_5 S_3 C_{45} + l_6 S_3 C_{456} - l_7 (C_7 S_3 C_{456} + C_3 S_7) - l_8 S_3 S_{456}$$

6.2 Inverse Kinematics

Inverse Kinematics Sagittal Plane:

The Fig. 6.2 shows the right leg in the Sagittal plane that describes the motion of the biped robot, where the base coordinate is at the center of the toe joint.

The position of the waist, the ankle and the toe are respectively (X_{3R}, Z_{3R}) , (X_{1R}, Z_{1R}) and (X_{0R}, Z_{0R}) .

Given the position of the hip and the ankle, the joint angle for the knee is calculated using the law of cosines to the triangle bounded by l_4 and l_5 :

$$C_{4R} = \frac{R^2 - l_4^2 - l_5^2}{2l_4^2 l_5^2}$$

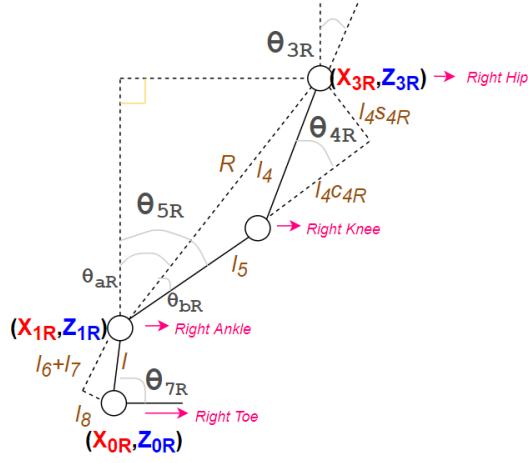


Figure 6.2. Sagittal Plane right leg

Using the trigonometric identity 'atan2' the knee angle is:

$$\theta_{4R} = \text{atan2}\left(\sqrt{1 - \left(\frac{R^2 - l_4^2 - l_5^2}{2l_4^2 l_5^2}\right)^2}, \frac{R^2 - l_4^2 - l_5^2}{2l_4^2 l_5^2}\right)$$

$$\text{Where } R^2 = (X_{3R} - X_{1R})^2 + (Z_{3R} - Z_{1R})^2$$

In order to calculate the ankle angle first the θ_{aR} and θ_{bR} are needed:

$$\theta_{aR} = \text{atan2}(X_{3R} - X_{1R}, Z_{3R} - Z_{1R})$$

$$\theta_{bR} = \text{atan2}(l_4 S_{4R}, l_5 + l_4 C_{4R})$$

$$\theta_{5R} = \theta_{aR} + \theta_{bR}$$

To keep the hip in a vertical position the sum of ankle, knee and hip angles need to be 0:

$$\theta_{3R} + \theta_{4R} + \theta_{5R} = 0$$

Thanks to this equation θ_{3R} is found.

Regarding the toe angle θ_{7R} :

$$\theta_{7R} = \text{atan2}\left(\frac{X_{3R} - X_{0R} - l_4 S_{4R} - l_5 S_{5R}}{l}, \frac{Z_{3R} - Z_{0R} - l_4 S_{4R} - l_5 S_{5R}}{l}\right)$$

$$\text{where } l = \sqrt{(l_6 + l_7)^2 + l_8^2}$$

For the left leg, following the same procedure:

$$\theta_{4L} = \text{atan2}\left(\sqrt{1 - \left(\frac{R^2 - l_4^2 - l_5^2}{2l_4^2 l_5^2}\right)^2}, \frac{R^2 - l_4^2 - l_5^2}{2l_4^2 l_5^2}\right)$$

$$\theta_{5L} = \theta_{aL} + \theta_{bL}$$

Where:

$$\theta_{aL} = \text{atan2}(X_{3L} - X_{1L}, Z_{3L} - Z_{1L})$$

$$\theta_{bL} = \text{atan2}(l_4 S_{4L}, l_5 + l_4 C_{4L})$$

$$\theta_{3L} = -\theta_{4L} - \theta_{5L}$$

$$\theta_{7L} = \text{atan2}\left(\frac{X_{3L} - X_{0L} - l_4 S_{4L} - l_5 S_{5L}}{l}, \frac{Z_{3L} - Z_{0L} - l_4 S_{4L} - l_5 S_{5L}}{l}\right)$$

Inverse Kinematics Frontal Plane:

The Fig. 6.3 shows the motion of the biped in the Frontal Plane, where θ_{6R} and θ_{6L} are the ankle angles and θ_{2R} and θ_{2L} are the hip angles, h represents the distance between the hip joints and the ankle joints, l_{step} is the width of a step.

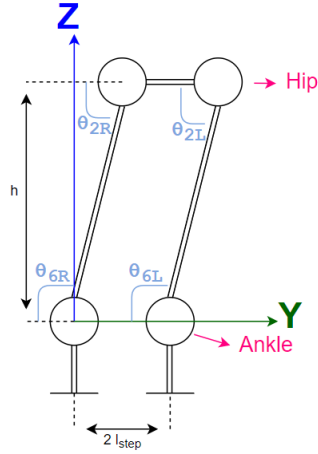


Figure 6.3. Frontal Plane

For the right leg:

Using the trigonometric identities:

$$\theta_{6R} = \frac{\pi}{2} + \text{atan2}(y - l_{step}, h)$$

In order to keep the hip in a vertical position:

$$\theta_{2R} + \theta_{6R} = \pi, \text{ using this equation } \theta_{2R} \text{ is found.}$$

For the left leg, using the same procedure:

$$\theta_{6L} = \frac{\pi}{2} + \text{atan2}(y - l_{step}, h)$$

$$\theta_{2L} + \theta_{6L} = \pi, \text{ using this equation } \theta_{2L} \text{ is found.}$$

Where y represents the trajectory followed by the hip joint which is a periodic function.

Part II

Chapter 7

Dataset

This chapter is partially done in collaboration with [1] and [2]. In order to simulate the kinematic an experimental protocol approved by the Institutional Review Board at the University of Texas at Dallas is used.

7.1 Incline Experiment

The IEEE Dataset presents ten subjects, they walk at steady speeds and inclines on a Bertec instrumented treadmill for one minute per trial. Each person can walk at three different speeds (0.8 m/s, 1 m/s, 1.2 m/s) and the inclination of the floor can be from -10 degrees to + 10 degrees at 2.5 degree increments, for a total of 27 trials.

During each trial, a 10-camera Vicon motion capture system recorded leg kinematics [4], while force plates in the Bertec treadmill recorded ground reaction forces [35] and [36], and a Delsys Trigno EMG system recorded muscle activation of the rectus femoris, biceps femoris, tibialis anterior, and gastrocnemius [37].

For marker signals the world frame is positioned at the base of the treadmill. This experiment's data is saved in two MATLAB structures, Continuous (the recording takes place normally and its progression is marked by the succession of temporal instants) and Gait-cycle (the recording is defined in terms of percentage with respect to the walking cycle).

Continuous

Subject details:

- Gender: 1 (male), 2 (female).
- Age: subject's age [years].
- Height: subject's height [mm].
- Weight: subject's weight [kg].
- Leg Length: subject's legs length [mm].

Trial details:

- Speed: treadmill's speed [m/s].
- Incline: treadmill's inclination [degrees].

Signals:

- Time in [s]
- Kinematics:
 - Markers: an array with world-frame positions of all motion-capture markers, located on ASI (Anterior Superior Iliac Spine), PSI (Posterior Superior Iliac Spine), the thigh, knee, tibia, ankle, heel, and toe of both legs. Results are split into three component directions: x, y, or z [mm].
 - Joint angles: an array with the joint angles for the pelvis, hip, knee, ankle and foot as calculated by Vicon Plug-in Gait (Vicon, Oxford, UK). Results are split into three component directions: x, y, or z [degrees].
- EMG data:
 - EMG sensors (Model:Trigno wireless system, Delsys, Natick, MA) are attached to the RF (rectus femoris), BF (biceps femoris), TA (tibialis anterior), and GC (gastrocnemius). The EMG signals have been rectified and low-pass filtered ($f_c = 40Hz$) with a zero-phase digital filter (MathWorks, Natick, MA) [V].
 - Accelerations: each Delsys EMG also contains a 3-axis accelerometer that reports an acceleration vector in the local frame. Results are split into three component directions: x, y, or z [m/s^2].
- Kinetics:
 - Joint power: array of the power generated by each joint, determined by Plug-In Gait (Vicon) [W/kg].
 - Joint force: array of the force applied at each joint, determined by Plug-In Gait (Vicon). Results are splitted into three component directions: x, y, or z [N/kg].
 - Joint moment: array of the moment generated by each joint, determined by Plug-In Gait (Vicon). Results are splitted into three component directions: x, y, or z [Nmm/kg].
 - Force-plate force: a 3D force vector from force plates in the split belt instrumented treadmill (Bertec, Columbus, OH). These signals have been low-pass filtered ($f_c = 40Hz$) with a zero-phase digital filter (MathWorks). Results are splitted into three component directions: x, y, or z [N].
 - Force-plate moment: a 3D moment vector from force plates in the split belt instrumented treadmill (Bertec). Results are splitted into three component directions: x, y, or z [Nmm].

- Force-plate cop: the center of pressure location (world-frame) from force plates in the split belt instrumented treadmill (Bertec). Results are splitted into three component directions: x, y, or z [mm].

Matlab organization: Continuous.(subject).(trial).(datatype).(leg).(variable)

- Subject (ABXX): ranges from 01 to 10, is the number of subjects.
- Trial:
 - subjectdetails (6x3cell):
 - * Gender (double).
 - * Age (double).
 - * Height (double).
 - * Weight (double).
 - * Left Leg Length (double).
 - * Right Leg Length (double).
 - (sXXi/dYY): XX is the speed of the trial (0x8, 1 and 1x2 [m/s]). YY is the incline of walking (10, 7x5, 5, 2x5 and 0 [degrees]), "i" stands for incline the "d" for decline.
- Datatype:
 - description (2x3cell):
 - * Speed (double).
 - * Incline (double).
 - kinematics :
 - * markers : cartesian signals (kinematiks.marker).
 - * jointangles: angular signals (kinematics.jointangles).
 - time (6000x1 double).
 - kinetics:
 - * jointpower: power generated signals (kinetics.jointpower).
 - * jointforce: applied force signals (kinetics.jointforce).
 - * jointmoment: moment generated signals (kinetics.jointmoment).
 - * forceplate: force plate signals (kinetics.forceplate).
 - emgdata:
 - * emg: EMG signals (emgdata.emg).
 - * accel: acceleration vector signals (emgdata.accel).

- Leg:
 - right: indicates the right leg.
 - left: indicates the left leg.
- Variable (depends on datatype, see Fig.7.1):
 - marker:
 - * asi (6000x3 double).
 - * psi (6000x3 double).
 - * thigh (6000x3 double).
 - * knee (6000x3 double).
 - * tibia (6000x3 double).
 - * ankle (6000x3 double).
 - * heel (6000x3 double).
 - * toe (6000x3 double).
 - joint:
 - * hip (6000x3 double).
 - * knee (6000x3 double).
 - * ankle (6000x3 double).
 - * pelvis (6000x3 double).
 - * foot (6000x3 double).
 - muscle:
 - * RF (6000x3 double for accelerations 6000x1 double for EMG).
 - * BF (6000x3 double for accelerations 6000x1 double for EMG).
 - * TA (6000x3 double for accelerations 6000x1 double for EMG).
 - * GC (6000x3 double for accelerations 6000x1 double for EMG).
 - forceplate:
 - * force (6000x3 double).
 - * moment (6000x3 double).
 - * cop (6000x3 double).

Gait cycle

For the gait cycle standard deviations and signal averages were also measured for all muscles considered for EMG, and for all spatial directions for all other kinematic and kinetic recordings.

Subject details:

- Gender: 1 (male), 2 (female).
- Age: subject's age [years].
- Height: subject's height [mm].
- Weight: subject's weight [kg].
- Leg Length: subject's legs length [mm].

Trial details:

- Speed: treadmill's speed [m/s].
- Incline: treadmill's inclination [degrees].

Signals:

- Steps out contains a vector of strides that we have identified to be outliers, as defined by having kinematics 3 standard deviations from the mean.
- Cycles time: array with the same dimensions as the other Gait Cycle data that indicates the time since the beginning of the corresponding stride [s].
- Cycles frame: vector that indicates what frame each heel strike occurred on.
- Kinematics:
 - Markers: array with world-frame positions of all motion-capture markers, located on the Anterior Superior Iliac Spine (asi), Posterior Superior Iliac Spine (psi), the thigh, knee, tibia, ankle, heel, and toe of both legs. Results are splitted into three component directions: x, y, or z [mm].
 - Joint angles: array with the joint angles for the pelvis, hip, knee, ankle, and foot as calculated by Vicon Plug-in Gait (Vicon, Oxford, UK). Results are splitted into three component directions: x, y, or z [degrees].
- EMG data:
 - EMG sensors (Model: Trigno wireless system, Delsys, Natick, MA) were attached to the rectus femoris (RF), biceps femoris (BF), tibialis anterior (TA), and gastrocnemius (GC). The EMG signals have been rectified and low-pass filtered ($f_c = 40Hz$) with a zero-phase digital filter (MathWorks, Natick, MA)[V].

-
- Accelerations: each Delsys EMG also contains a 3-axis accelerometer that reports an acceleration vector in the local frame. Results are splitted into three component directions: x, y, or z [m/s^2].
 - Kinetics:
 - Joint power: array of the power generated by each joint, determined by Plug-In Gait (Vicon) [W/kg].
 - Joint force: array of the force applied at each joint, determined by Plug-In Gait (Vicon). Results are splitted into three component directions: x, y, or z [N/kg].
 - Joint moment: array of the moment generated by each joint, determined by Plug-In Gait (Vicon). Results are splitted into three component directions: x, y, or z [Nmm/kg].
 - Force-plate force: 3D force vector from force plates in the split belt instrumented treadmill (Bertec, Columbus, OH). These signals have been low-pass filtered ($f_c = 40Hz$) with a zero-phase digital filter (MathWorks). Results are splitted into three component directions: x, y, or z [N].
 - Force-plate moment: a 3D moment vector from force plates in the split belt instrumented treadmill (Bertec). Results are splitted into three component directions: x, y, or z [Nmm].
 - Force-plate cop: the CoP location (world-frame) from force plates in the split belt instrumented treadmill (Bertec). Results are splitted into three component directions: x, y, or z [mm].

Matlab organization: Gaitcycle.(subject).(trial).(datatype).(leg).(variable)

- subject (ABXX): ranges from 01 to 10, is the number of subjects.
- trial:
 - subjectdetails (6x3cell):
 - * Gender (double).
 - * Age (double).
 - * Height (double).
 - * Weight (double).
 - * Left Leg Length (double).
 - * Right Leg Length (double).
 - (sXXi/dYY): XX is the speed of the trial (0x8, 1 and 1x2 [m/s]). YY is the incline of walking (10, 7x5, 5, 2x5 and 0 [degrees]), "i" stands for incline the "d" for decline.

- datatype:
 - description (2x3cell):
 - * Speed (double).
 - * Incline (double).
 - kinematics:
 - * markers : cartesian signals (kinematiks.marker).
 - * jointangles: angular signals (kinematics.jointangles).
 - stepsout: vector of strides that we have identified to be outliers.
 - cycle:
 - * time (cycles.time, $150 \times M^3$ double).
 - * frame (cycles.frame, $1 \times (M + 1)$ double).
 - kinetics:
 - * jointpower: power generated signals (kinetics.jointpower).
 - * jointforce: applied force signals (kinetics.jointforce).
 - * jointmoment: momente generated signals (kinetics.jointmoment).
 - * forceplate: force plate signals (kinetics.forceplate).
 - emg-data:
 - * emg: EMG signals (emgdata.emg).
 - * accel: acceleration vector signals (emgdata.accel).
- Leg:
 - right: indicates the right leg.
 - left: indicates the left leg.
- Variable (depends on datatype, see Fig.7.2):
 - marker:
 - * asi (150xM double for the three component directions 150x1 double for mean and standard deviation).
 - * psi (150xM double for the three component directions 150x1 double for mean and standard deviation).
 - * knee (150xM double for the three component directions 150x1 double for mean and standard deviation).
 - * tibia (150xM double for the three component directions 150x1 double for mean and standard deviation).
 - * ankle (150xM double for the three component directions 150x1 double for mean and standard deviation).
 - * heel (150xM double for the three component directions 150x1 double for mean and standard deviation).

- * toe (150xM double for the three component directions 150x1 double for mean and standard deviation).
- joint:
 - * hip (150xM double for the angular position 150x1 double for mean and standard deviation).
 - * knee (150xM double for the angular position 150x1 double for mean and standard deviation).
 - * ankle (150xM double for the angular position 150x1 double for mean and standard deviation).
 - * pelvis (150xM double for the angular position 150x1 double for mean and standard deviation).
 - * foot (150xM double for the angular position 150x1 double for mean and standard deviation).
- muscle:
 - * RF (150xM double for the three component directions and EMG 150x1 double for mean and standard deviation).
 - * BF (150xM double for the three component directions and EMG 150x1 double for mean and standard deviation).
 - * TA (150xM double for the three component directions and EMG 150x1 double for mean and standard deviation).
 - * GC (150xM double for the three component directions and EMG 150x1 double for mean and standard deviation).
- force-plate:
 - * force (150xM double for the three component directions 150x1 double for mean and standard deviation).
 - * moment (150xM double for the three component directions 150x1 double for mean and standard deviation).
 - * cop (150xM double for the three component directions 150x1 double for mean and standard deviation).

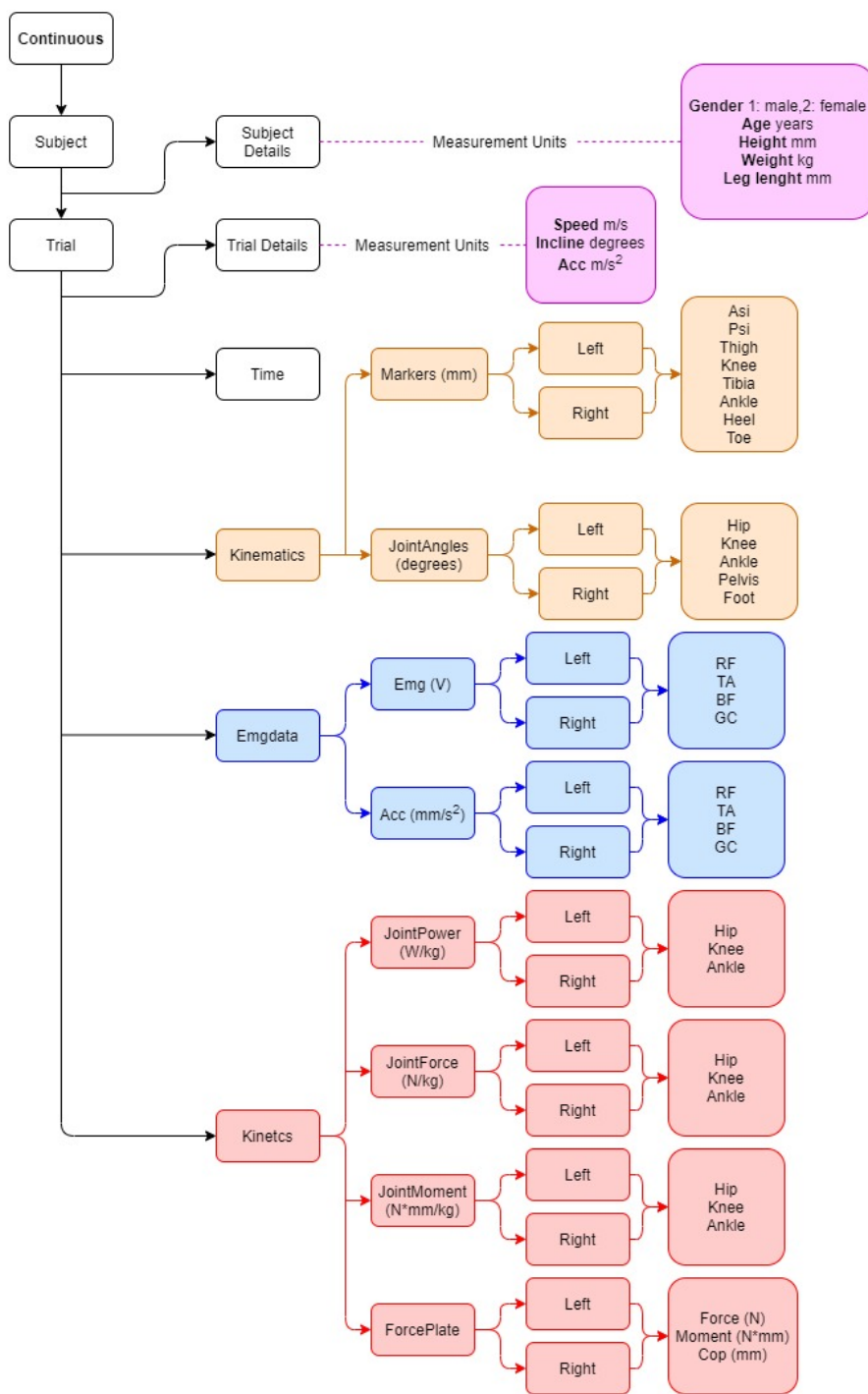


Figure 7.1. Continuous data Hierarchy

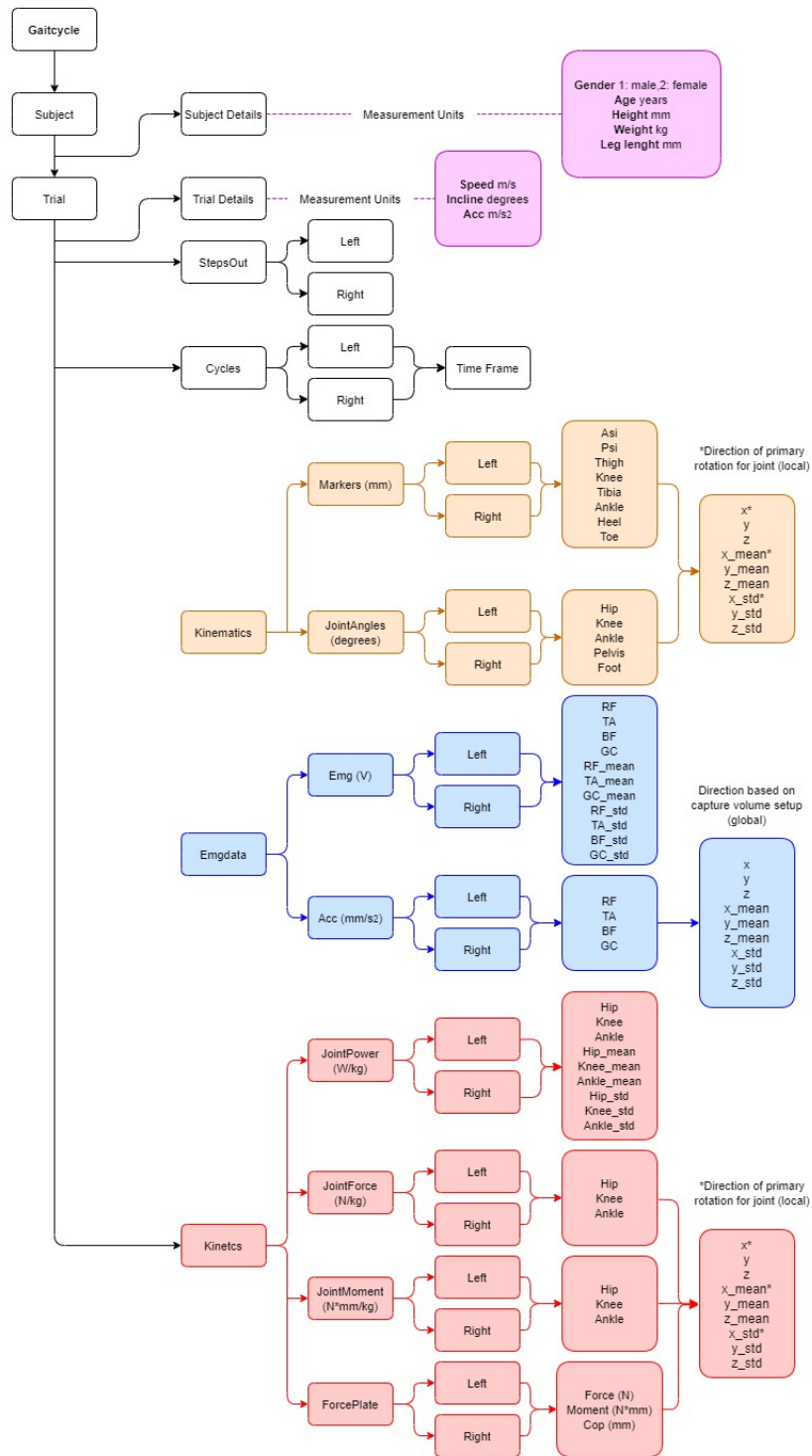


Figure 7.2. Gait cycle data Hierarchy

Chapter 8

Simulation on Matlab: data analysis and variables generation

In this chapter is presented the simulation and the study done on Matlab, this is done in collaboration with the study made by [1] and [2] but in this thesis another subject is used. In order to simulate correctly the biped kinematics during the gait the following input variables are needed: CoG and meta trajectories (they are the projection of the ankle on the ground), feet and trunk angles wrt the ground plane and also the respective speeds. The first step consists in obtaining the ZMP trajectory from the gait events and the feet and steps characteristics. The gait events are four and are recognized with a state-machine and determined from the feet markers contained in the dataset. In particular the feet markers gave the step length and width, the feet plant and dorso dimensions.

Thanks to the feet events it was possible to determine the motion of the feet meta (position in time and their angles wrt the ground) [3]. From the ZMP trajectory, according to the LIMP model theory by [4], were computed the CoM position and speed. Finally, the trajectories and speed variables were packed together to be used in the kinematics cycle. In this and the following chapter there are a series of graphs, tables of values and data. They all refer to the experimental data (InclineExperiment.mat) for subject AB07 during the trial s1i0, with the treadmill not inclined and a walking speed of 1 m/s.

8.1 Data analysis

The simulations are done using Matlab. Thanks to the foot marker data, the different walking events at which support point (heel or toe) and consequently the support leg (left or right) change were detected.

In order to detect the support state during the trial a simple state machine was developed Fig. 8.1. It has two states variables: the stance leg (left or right) and the stance point (toe or heel).

The combination of these two states determine four phases: *left tip support*, *right heel support*, *right tip support*, *left heel support*.

The events that must occur in order to change state are:

- Change of support point:
when $Z_{stancefootT} \geq Z_{stancefootH}$ the support point is changing from the heel to the tip of the stance foot.
- Change of support leg:
if there is a local minimum of $Z_{swingingfootH}$ while standing on the tip of the opposite foot it corresponds to a heel-strike of the swinging foot. The support leg changes, as well the support point, and a step was completed.

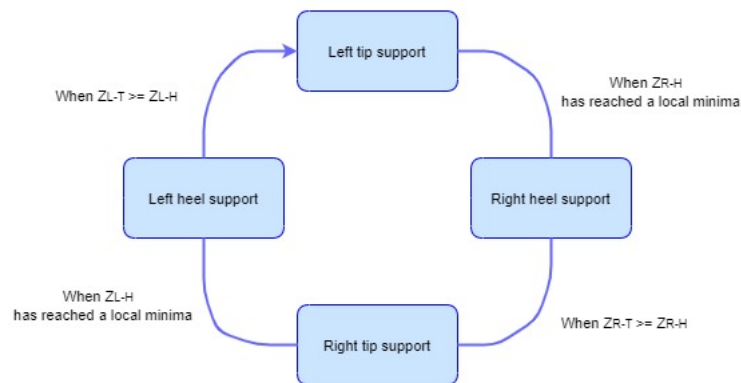


Figure 8.1. State machine

The first state is determined from the different $Z_{foot-point}$ time plots, it depends on smallest of the values, while the other depends on the events. Sometimes the subject walks without touching the heel to the ground. However $Z_{swingingfootH}$ has a local minimum also in this case, so a short period of heel support will always be considered before switching to the tip support state, even if only for one sample. Additionally, the condition for the first event makes it possible to change the support point even if the heel and the tip do not lie together on the ground for a moment. The double support period corresponds to the time spent in heel support, while the single support period corresponds to the time passed in toe stance, in the case of a slow walk. Thus it is possible not only to determine the stance leg and the support point but also if the subject is in double or single stance. The Fig.8.2 represents the heel and toe marker's position along the Z axis.

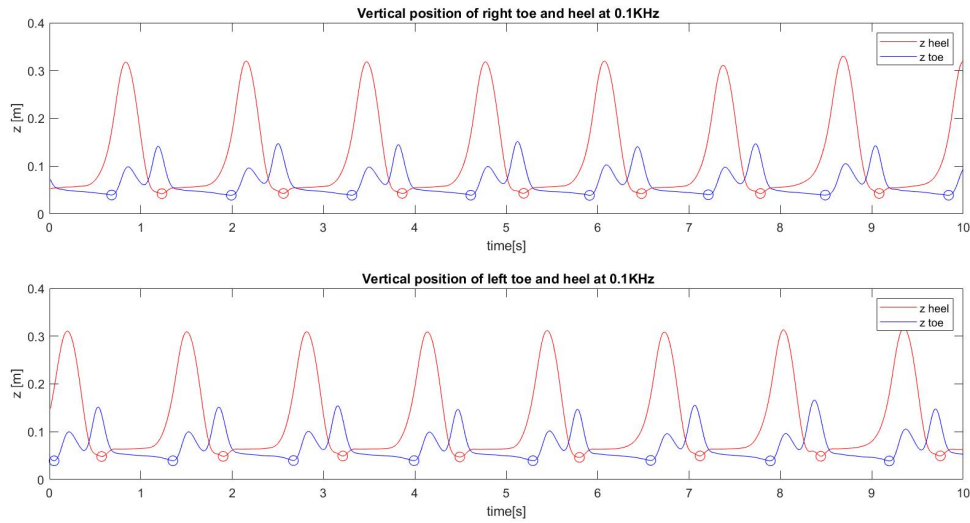


Figure 8.2. Heel and toe markers position along the axis z for the subject AB07 and trial s1i0. The minimum are highlighted with the circle

At the end of this process is generated an array (*supportinfos*) containing a series of structures with the following informations:

- Stance Leg
- Support Point
- Step Number
- Start Time
- End Time
- Stance: this is an array providing the current state of support
- Time array of the period

Using the array *supportinfos* is possible to segment the data according to the state of the support.

In the gait analysis it is important to know the correct lengths of the body segments, as well as the position of the joint centers. Due to the lack of measurements on the lower limb segments, their length were calculated from the markers, following the procedure given by the Vicon Plug-in Gait Reference guide [5]. The Newington-Cage [6] model is used to define the positions of the hip joint centers in the pelvis segment. The interAsis distance is computed as the value between the left ASI (LASI) and the right ASI (RASIS) markers. The distances from the Asis to the Trochanter are calculated independently for

each leg, using the following formula (8.1):

$$AsisTrocDist = 0.1288LegLength - 48.56 \quad (8.1)$$

The offsets vectors for the left hip joint center (LHJC) and the right one (RHJC) are calculated as follow (8.2)(8.3)(8.4):

$$X = C \cos \theta \sin \beta - (AsisTrocDist + mm) \cos \beta \quad (8.2)$$

$$Y = -(C \sin \theta - aa) \quad (8.3)$$

$$Z = -C \cos \theta \cos \beta - (AsisTrocDist + mm) \sin \beta \quad (8.4)$$

where:

C is $0.115\text{MeanLegLength}-15.3$

aa is the interAsis distance

θ is taken as 0.5 rad

β is taken as 0.314 rad

For the right joint center, the Y is negated, since Y is in the lateral direction for the pelvis embedded coordinate system. In order to define the joint centers of the ankles (AJC) and knees (KJC) is developed a function called chord. A plane is defined from a set of three points: calculated joint center, the required joint center and marker attached to the body segments that links them Fig. 8.3. The joint center required is located perpendicular to the respective joint marker at a certain distance (joint center offset).

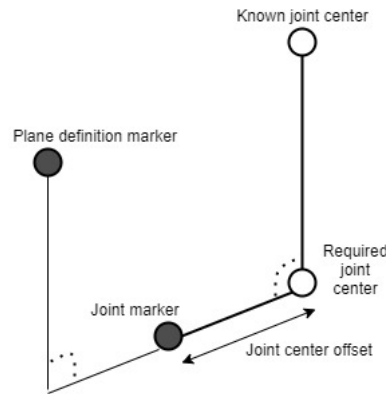


Figure 8.3. Relationship between two successive joint centers and related markers

As described by [1] the KJC and AJC can be calculated by adding half the measured joint width and respective joint marker diameter. This function is called chord because the three points (two joint centers and the joint marker) lie on the periphery of the same circle. In the function chord the joint markers lie in the same plane of the two joint centers and the plane definition marker. A modified version of the function calculates the required joint center position when the plane definition marker is rotated out of this plane by a known angle around the proposed joint center axis. After positioning the joint centers, the length of the body segments can be determined. The pelvis segment is between the two HJCs, the femur segment goes from the HJC to the KJC, while the tibial goes from the KJC to the AJC. The foot plant is represented by the segment between the heel and the toe markers, while the foot dorso is the segment which links the AJC and the toe marker. Projecting the AKJ on the foot plant the meta position is obtained. Considering that each body segment can be represented by a vector connecting two successive joints, and that a joint rotates two segments one w.r.t. the other, the rotation around a particular joint center can be calculated from the relative orientation of the vectors starting from that joint. Let be a and b the unit vectors representing the orientation of two consecutive body segment vectors linked by a joint. The rotation matrix R representing their relative orientation can be calculated as (8.5):

$$R = I + [v]_{skew} + [v]_{skew}^2 \frac{1 - c}{s^2} \quad (8.5)$$

where:

$$v = a \times b \quad (8.6)$$

$$s = \|v\| \quad (8.7)$$

$$c = a \cdot b \quad (8.8)$$

$$[v]_{skew} = \begin{bmatrix} 0 & -v_3 & v_2 \\ v_3 & 0 & -v_1 \\ -v_2 & v_1 & 0 \end{bmatrix} \quad (8.9)$$

From the rotation matrix it is possible to compute the relative angles, computed with an appropriate MATLAB function described by the Algorithm 1 Fig. 8.4.

```

Data:  $R_{(3 \times 3)}$ 
Result:  $\varphi, \vartheta, \psi$ 
if  $R_{3,1} \neq 1$  and  $R_{3,1} \neq -1$  then
     $\psi_1 = -\arcsin R_{3,1}$ ;
     $\psi_2 = \pi - \arcsin R_{3,1}$ ;
     $\varphi_1 = \text{Atan2}(R_{3,2}/\cos \psi_1, R_{3,3}/\cos \psi_1)$ ;
     $\varphi_2 = \text{Atan2}(R_{3,2}/\cos \psi_2, R_{3,3}/\cos \psi_2)$ ;
     $\vartheta_1 = \text{Atan2}(R_{2,1}/\cos \psi_1, R_{1,1}/\cos \psi_1)$ ;
     $\vartheta_2 = \text{Atan2}(R_{2,1}/\cos \psi_2, R_{1,1}/\cos \psi_2)$ ;
     $\psi = \min(\psi_1, \psi_2)$ ;
     $\varphi = \min(\varphi_1, \varphi_2)$ ;
     $\vartheta = \min(\vartheta_1, \vartheta_2)$ ;
else
     $\vartheta = 0$ ;
    if  $R_{3,1} = -1$  then
         $\psi = \pi/2$ ;
         $\varphi = \vartheta + \text{Atan2}(R_{1,2}, R_{1,3})$ ;
    else
         $\psi = -\pi/2$ ;
         $\varphi = -\vartheta + \text{Atan2}(-R_{1,2}, -R_{1,3})$ ;
    end
end

```

Algorithm 1: Computing rotation angles from a given rotation matrix R.

Figure 8.4. Algorithm 1

To use the chord or modified one, functions require the value of the joint center offsets or at least the diameter of the articulations, but these are not present in the experimental data. For this reason we opted for a trial and error process using chords, thus assuming that the joint marker is not rotated w.r.t. the plane defined by the joint centers and their respective plane definition marker. First an appropriate value of the joint offsets is established and second the joint angles computed using the method presented above to those from the dataset are compared. If they coincide, the joint offsets were accepted as valid. This method gave acceptable results, and the body segments found is Fig.8.5.

Outputs

The extension of the left and right tibial segment, the femur segment, the foot plant, and the segment between the HJCs is calculated at each instant. The time-averaged length of each body segment was determined, and the standard deviation of each time sample. To establish if the joint offsets values were chosen properly the standard deviations must not exceed a certain threshold: in that case there the lengths vary excessively over time. In any case, it is impossible to obtain the time invariant length of the body segments, because of the same measurement methodology. The motion capture system may not measure the position of the markers correctly, and markers may shift during walking. There will always be a few values that deviate significantly from the average, even in the best situation. The mean values of the body segment lengths are packed in the structure *meanLength*. The state machine output *supportinfos* contains the time limits of each period that the subject spends with a certain support. These were used to segment the continuous records of the joint variables and of the marker coordinates, obtaining the structure arrays *jointinfos* and *markerinfos*.

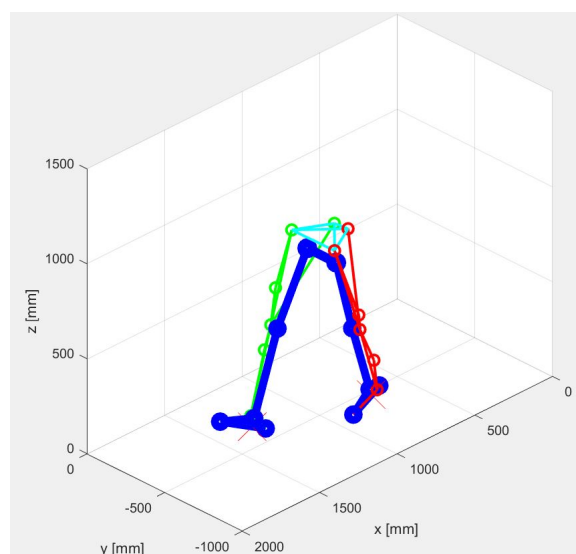


Figure 8.5. Markers and body segments

These were packed together with *supportinfos* in the structure variable *segmentedData*. The time continuous variables of the joint and the marker, were grouped in *completeTrial*.

Table 8.1. Chosen center offsets for the subject AB07 and trial s1i0

JOINT	JOINT OFFSET
Left and right KJC	38mm
Left and right AKJ	35mm

8.2 Cartesian variables generation

As described by [1] and [2] in this section is presented both the ZMP and feet trajectories generation and the CoG computation using Matlab.

8.2.1 ZMP and feet trajectories generation

The aim of this part is to describe the trajectories of the ZMP and the meta of the feet using the variables obtained as output from the previous part. First of all, the incomplete steps were deleted from the recordings, to start and end the trial with a flat-foot event. Then, starting from the first flat-foot event of the trial, the following parameters are found iteratively:

- stepN : step number.
- t_{to} : time between at-foot and toe-off events of the support foot.
- t_{hs} : time between toe-off and the heel-strike events of the support foot.
- t_{ff} : time between heel-strike and at foot events of the support foot.
- Δx_{step} : the longitudinal distance between the meta of the feet, calculated at the at-foot event.
- Δy_{step} : the lateral distance between the meta of the feet, calculated at the at-foot event.
- l_f : the longitudinal distance between the markers of the meta and of the toe of the supporting foot during the at-foot event. Constant parameter because it depends only on the length of the foot.
- l_b : the longitudinal distance between the markers of the meta and of the heel of the supporting foot during the at-foot event. Constant parameter because it depends only on the length of the foot.

ZMP generation from the support states

In flat-footed walking, the ZMP remains fixed in the middle of the sole of the supporting foot until it moves to the opposite foot during the double stance phase. The ZMP longitudinal trajectory between two flat-footed events occurring at time t_i and time t_f respectively is given by:

$$ZMP_x(t) = \begin{cases} ZMP_x(t_i) + (l_f/t_{ff})t, & t_i < t \leq t_i + t_{ff} \\ ZMP_x(t_i) + (l_b/t_{to})t - l_b + \Delta x_{step}, & t_i + t_{ff} < t \leq t_f \end{cases} \quad (8.10)$$

For the lateral direction:

$$ZMP_y(t) = \begin{cases} \Delta y_{step}, & t_i < t \leq t_i + t_{ff} \\ (K_f - K_y)t/t_{to} - K_f, & t_i + t_{ff} < t \leq t_f \end{cases} \quad (8.11)$$

Where:

$$K_y = \frac{\Delta y_{step} \omega_n \tanh(\omega_n(t_{to}))}{1 + \Delta y_{step} \omega_n \tanh(\omega_n(t_{to}))} \quad (8.12)$$

ω_n is the natural frequency of the inverted pendulum and it is defined as $\omega_n = \sqrt{g/z_{CoG}}$ [3]. K_f equal to K_y calculated for the next step. At this point the ZMP position is compared with the CoP data measured by the two force plates placed under the Bertec treadmill used in the trials Fig. 8.6 - 8.7. The comparison shows that the calculated ZMP has a similar trend to that of the CoP in the longitudinal direction x and they almost overlap completely. In the lateral direction y, however, the situation is different: the lines parallel to the time axis of the ZMP and those of the CoP corresponding to the single support phase do not coincide. This occurs for two reasons: during the double stance phase, force platforms are unable to measure the displacement of the CoP from one foot to the other, and during the single stance phases, the CoP moves from the inner part of the sole to the outer part due to the pronation of the stance foot. The double stance phases correspond to the intervals between a heel-strike event and a flat foot event of the same foot. The generated trajectory of the ZMP can be seen as a continuous piecewise linear function. Its break-points have been recorded to be used in the CoG generation process to compute the angular coefficients of the ZMP linear traits.

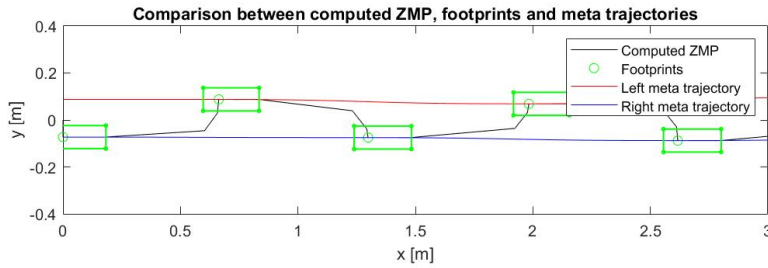


Figure 8.6. Comparison between computed ZMP footprints and meta trajectories.

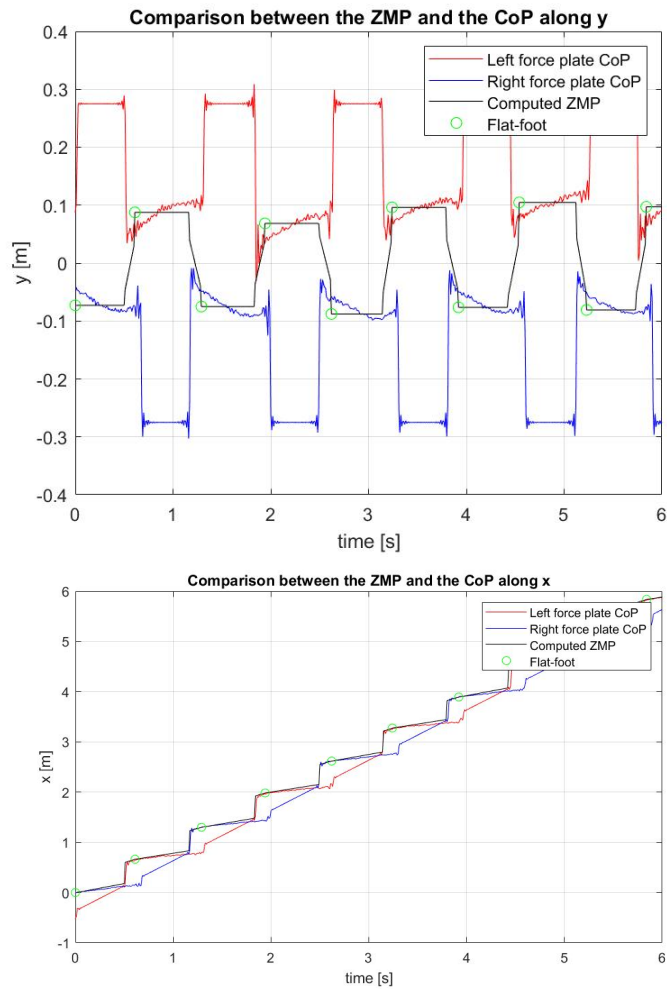


Figure 8.7. Comparison between the generated ZMP (black line) and the CoPs (blue and red lines) taken from experimental data along the lateral direction and the longitudinal lateral direction.

Outputs

The outputs of the processes defined previously in the section are the ZMP trajectory, the meta trajectories and the angles of the feet w.r.t. the ground. To these variables a first trait was added to simulate the transition from standing with both feet touching the ground to the first half-step. This ensures that the biped starts from a stable position. The recorded ZMP break-points are collected to be used for reconstructing the continuous piecewise linear function which matches the ZMP trajectory.

8.2.2 CoG computation

In order to compute the CoG trajectory and to verify the proper ZMP tracking, the method proposed by Russ Tedrake [4] is used; he proposes an iterative method for finding solutions to the LQR problem. The state space form for CoM and ZMP is:

$$\dot{x} = Ax + Bu = \begin{bmatrix} 0_{2 \times 2} & I_{2 \times 2} \\ 0_{2 \times 2} & 0_{2 \times 2} \end{bmatrix} x + \begin{bmatrix} 0_{2 \times 2} \\ I_{2 \times 2} \end{bmatrix} u \quad (8.13)$$

$$\dot{y} = Cx + Du(x, u) = \begin{bmatrix} I_{2 \times 2} & 0_{2 \times 2} \end{bmatrix} x + \frac{-z_{CoM}}{\ddot{z}_{CoM}} I_{CoM} u \quad (8.14)$$

where:

$$x = \begin{bmatrix} x_{CoG} \\ \dot{x}_{CoG} \\ x_{CoG} \\ \dot{x}_{CoG} \end{bmatrix}, u = \begin{bmatrix} \ddot{x}_{CoG} \\ \ddot{x}_{CoG} \end{bmatrix}, y = \begin{bmatrix} x_{ZMP} \\ x_{ZMP} \end{bmatrix} \quad (8.15)$$

Assuming a constant z_{CoG} , $D(x,u)$ becomes $D(u)$. The ZMP trajectories $y_d(t)$ can be described by a continuous polynomial:

$$y_d(t) = \sum_k^{i=0} c_{j,i} (t - t_j)^i \quad \text{for } j = 0, \dots, n-1 \text{ and } \forall t \in [t_j, t_{j+1}] \quad (8.16)$$

Given $y_d(t)$ the optimal ZMP tracking controller can be obtained solving a continuous-time LQR problem:

$$\begin{aligned} & \text{Minimize } u(t) \quad \int_0^{inf} g(\bar{x}(t), u(t)) dt \\ & \text{Subject to} \quad Q = Q^T > 0 \\ & \quad \quad \quad R = R^T > 0 \\ & \quad \quad \quad y_d(t) = y(t_f) \quad \forall t \geq t_f \\ & \quad \quad \quad \dot{x}(t) = Ax(t) + Bu(t) \\ & \quad \quad \quad y(t) = Cx(t) + Du(t) \end{aligned} \quad (8.17)$$

and initial conditions $x(0) = x_0$. Q and R explicitly trade off ZMP tracking performance against the cost of accelerating the CoG. Note that Q has to be positive defined. In 8.17:

$$g(\bar{x}(t), u(t)) = \bar{x}^T Q_1 \bar{x} + \bar{x}^T q_2(t) + q_3(t) + u^T(t) R_1 u(t) + u^T(t) r_2(t) + 2\bar{x}^T(t) N u(t) \quad (8.18)$$

where:

$$\begin{aligned} Q_1 &= C^T Q C; & q_2(t) &= -2C^T Q \bar{y}_d(t); & q_3 &= \|\bar{y}_d(t)\|_Q^2; \\ R_1 &= R + D^T Q D; & r_2(t) &= -2D Q \bar{y}_d(t); & N &= C^T Q D \end{aligned} \quad (8.19)$$

The optimal cost-to-go for this problem has the general form:

$$J(\bar{x}(t), t) = \bar{x}^T(t) S_1(t) \bar{x}(t) + \bar{x}^T(t) s_2(t) + s_3(t) \quad (8.20)$$

The optimal controller is defined as:

$$u^*(t) = -R_1 (N \bar{x}(t) + r_s(t)) \quad (8.21)$$

where:

$$N_B = N^T + B^T S_1 \quad r_s = \frac{1}{2}(r_2(t) + B^T s_2) \quad (8.22)$$

After some considerations the optimal feedback controller can be expressed as:

$$u^*(t) = K_1 \bar{x}(t) + k_2(t) \quad (8.23)$$

where the feedback matrix K_1 is a constant and:

$$k_2(t) = -R_1^{-1} \left(\frac{1}{2} B^T s_2(t) - DQ\bar{y}_d(t) \right) \quad (8.24)$$

The solution to this systems:

$$z(t) = e^{A_z(t-t_j)} a_j + \sum_{i=0}^k b_{j,i}(t-t_j)^i \quad (8.25)$$

In order to solve the coefficients of 8.25 the following algorithm can be used: *Outputs*

Data: $x(0)$, A_z , B_z , degree k piecewise polynomial $\bar{y}_d(t)$ with n breaks

Result: a_j , $b_{j,i}$, $\forall j \in (1, \dots, n)$, $\forall i \in (0, \dots, k)$

for $j = n, \dots, 1$ **do**

$\beta_{j,k} = -A_z^{-1} B_z c_{j,k}$;

for $i = k-1, \dots, 0$ **do**

$b_{j,i} = A_z^{-1} ((i+1)b_{j,i+1} - B_z c_{j,i})$;

end

$a_j = \begin{bmatrix} x - b_{j,1} \\ \alpha_j \end{bmatrix}$;

$x = \begin{bmatrix} I \\ 0 \end{bmatrix} e^{A_z(t_{j+1}-t_j)} a_j + \sum_{i=0}^{k-1} b_{j,i}(t_{j,i} - t_i)^i$;

end

$b_{j,1}[1:2] = b_{j,1}[1:2] + y(t_j)$;

Using the following gains:

$$Q = \begin{bmatrix} 100 & 0 \\ 0 & 100 \end{bmatrix} \quad R = \begin{bmatrix} 0.01 & 0 \\ 0 & 0.01 \end{bmatrix} \quad (8.26)$$

The Fig.8.8-8.9 are obtained.

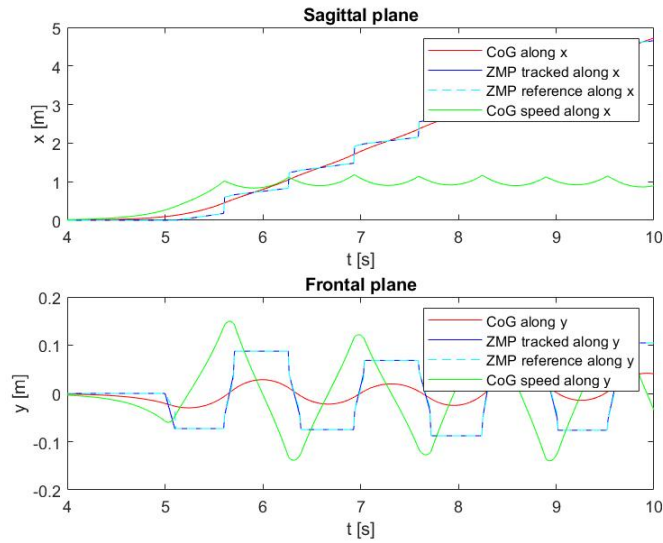


Figure 8.8. Comparison of the reference and tracked ZMP with the generated CoG along x and y

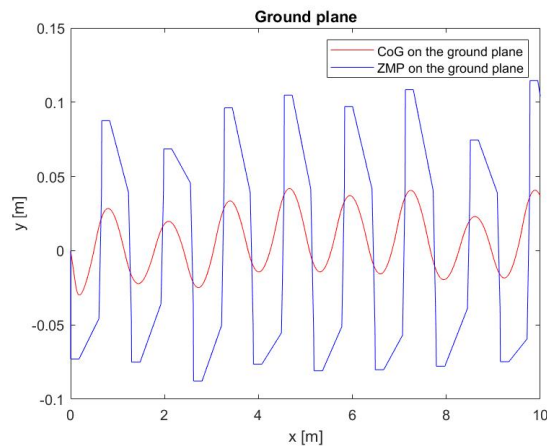


Figure 8.9. Comparison between CoG and ZMP on the xy ground plane

The reference ZMP was perfectly tracked thanks to the use of a rather large time horizon of about sixty seconds. The longer the reference ZMP, the more accurate the tracking. The motion of the CoG is stable, and never moves outside the line traced by the ZMP, except during the first half step. Along the longitudinal direction its trajectory seems a straight line, while in the lateral a sine wave which peaks approach the ZMP during the single support phase. The velocity of the CoG along x starts from zero, increases, and then begins to oscillate around a constant value, equal to the trial's walking speed,

reported in the experimental data. Instead the CoG's speed along y is represented by a triangular wave with rounded edges, and reach is peak during the double support phase, when the position of the CoG passes from one side the other.

8.3 Kinematic model

As described by [1] and [2] in this section is presented both the Direct kinematics and the Inverse kinematics procedures used then on Matlab.

8.3.1 Direct kinematics

The direct kinematics is a function $K(\theta)$ that relates the linear and angular displacements of the model in the Cartesian space to its configuration, i.e. the set of its joint angles θ . Direct kinematics creates a link between joint space variables θ and Cartesian space variables x .

$$x = K(\theta) \quad (8.27)$$

Consider two reference systems RF_0 , RF_1 , and an arbitrary point P in space. Let p_0 be the vector of coordinates of P w.r.t. the reference frame RF_0 . Instead let p_1 be the vector representing the position of P w.r.t. RF_1 . Let $d_{(0 \rightarrow 1)}$ be the distance of the origin of RF_1 from the origin of RF_0 , and $R_{(0 \rightarrow 1)}$ be the rotation matrix of RF_1 with respect to RF_0 . The position p_0 of P in RF_0 is given by:

$$p_0 = d_{(0 \rightarrow 1)} + R_{(0 \rightarrow 1)}p_1 \quad (8.28)$$

Fig.8.28 represents the coordinate transformation (translation + rotation) of a bound vector between two frames. After the computation of the homogeneous transformation matrix $T_{(0 \rightarrow 1)}$, that gives us all the information needed to describe the direct kinematics: it is a suitable instrument for describing the orientation and position of a body in space w.r.t a reference frame, in terms of its ZYX angles ϕ (calculated from R) and its translation vector p , giving all the Cartesian space variables x :

$$x = \begin{bmatrix} \theta \\ p \end{bmatrix} = \begin{bmatrix} \psi \\ \theta \\ \phi \\ p_x \\ p_y \\ p_z \end{bmatrix} \quad (8.29)$$

Then is computed the homogeneous transformations of the reference frames of the meta of the supporting foot (F_1), of the model's CoG and of the meta of the swinging foot (F_2). These are obtained by the product of a series of homogeneous transformations starting from the base frame (i.e. the Cartesian reference system) to the corresponding point:

$$\begin{aligned} T_{(0 \rightarrow F_1)} &= T_{(0 \rightarrow 1)}T_{(1 \rightarrow 2)}T_{(2 \rightarrow 3)}T_{(3 \rightarrow F_1)} \\ T_{(0 \rightarrow CoG)} &= T_{(0 \rightarrow 3)}T_{(3 \rightarrow 4)}T_{(4 \rightarrow 5)}T_{(5 \rightarrow 6)}T_{(6 \rightarrow 7)}T_{(7 \rightarrow 8)}T_{(8 \rightarrow 9)}T_{(9 \rightarrow CoG)} \\ T_{(0 \rightarrow F_2)} &= T_{(9 \rightarrow 10)}T_{(10 \rightarrow 11)}T_{(11 \rightarrow 12)}T_{(12 \rightarrow 13)}T_{(13 \rightarrow 14)}T_{(14 \rightarrow 15)}T_{(15 \rightarrow F_2)} \end{aligned} \quad (8.30)$$

Given a model such as those defined in the previous section, we consider fixed the support point of the foot until it is changed. In each joint and point of interest there's a local frame, like described in the previous section. The value 0 indicates the reference frame located on the support point and attached to the terrain, while the other numbers indicate the other reference frames located on the joints. Each of these, except the last of each formula in 8.30 $T_{(3 \rightarrow F_1)}$, $T_{(9 \rightarrow CoG)}$ which are constant transformation, $T_{(15 \rightarrow F_2)}$, depends on the i -th joint angle. Thus the position of F_1 depends only on the angles of the support foot w.r.t. the ground. Instead F_2 and CoG position depends also on the other joint variables.

8.3.2 Inverse kinematics

The differential inverse kinematics gives the following relationship:

$$\dot{x} = J_A(\theta)\dot{\theta} \quad (8.31)$$

where J_A is the analytical Jacobian and is expressed by:

$$J_A(\theta) = \frac{\partial K(\theta)}{\partial \theta} \quad (8.32)$$

Given a set of three linear and three angular velocities (\dot{p} and $\dot{\phi}$) to be computed, the analytical Jacobian is a 6x6 matrix such that:

$$\dot{x}_{ref} = \begin{bmatrix} \dot{\phi} \\ \dot{p} \end{bmatrix} = \begin{bmatrix} J_{\phi}(\theta) \\ J_p(\theta) \end{bmatrix} = J_A(\theta)\dot{\theta} \quad (8.33)$$

This formula represents the linear relationship between the velocities in Cartesian space and those at the joints. The aim is to track precisely the motion of the CoG, of F_1 and F_2 , the orientation and position of their reference frames in space, and how their time evolves. Their Cartesian linear and rotational velocities are grouped within the vector \dot{x}_{ref} , the vector of the reference speeds. The differential direct kinematic that gives the set of reference variables x_{ref} can be written as follows:

$$\dot{x}_{ref} = \begin{bmatrix} \dot{\phi}_{CoG} \\ \dot{p}_{CoG} \\ \dot{\phi}_{F_1} \\ \dot{\phi}_{F_2} \\ \dot{p}_{F_2} \end{bmatrix} = J_{A(15 \times 15)}(\theta) \begin{bmatrix} \dot{\theta}_{1-F_1} \\ \dot{\theta}_{2-F_1} \\ \dot{\theta}_{3-F_1} \\ \dot{\theta}_{1-Ankle_1} \\ \dot{\theta}_{2-Ankle_1} \\ \dot{\theta}_{Knee_1} \\ \dot{\theta}_{1-Hip_1} \\ \dot{\theta}_{2-Hip_1} \\ \dot{\theta}_{3-Hip_1} \\ \dot{\theta}_{3-Hip_2} \\ \dot{\theta}_{2-Hip_2} \\ \dot{\theta}_{1-Hip_2} \\ \dot{\theta}_{Knee_2} \\ \dot{\theta}_{2-Ankle_2} \\ \dot{\theta}_{1-Ankle_2} \end{bmatrix} \quad (8.34)$$

where:

$$J_{A(15 \times 15)}(\theta) = \begin{bmatrix} J_{\phi CoG}(\theta) \\ J_{pCoG}(\theta) \\ J_{\phi F_1}(\theta) \\ J_{\phi F_2}(\theta) \\ J_{pF_2}(\theta) \end{bmatrix} \quad (8.35)$$

To obtain the redundancy of constraints, the number of dof has to be lower than the reference variables. Constraints can be added in both joint space and Cartesian space. The knee angles were added on the left side of Eq.8.34 as additional reference variable, obtaining:

$$\begin{bmatrix} \dot{\phi}_{CoG} \\ \dot{p}_{CoG} \\ \dot{\phi}_{F_1} \\ \dot{\phi}_{F_2} \\ \dot{p}_{F_2} \\ \dot{\theta}_{Knee1} \\ \dot{\theta}_{Knee1} \end{bmatrix} = J_{A(17 \times 15)}(\theta) \begin{bmatrix} \dot{\theta}_{1-F_1} \\ \dot{\theta}_{2-F_1} \\ \dot{\theta}_{3-F_1} \\ \dot{\theta}_{1-Ankle1} \\ \dot{\theta}_{2-Ankle1} \\ \dot{\theta}_{Knee1} \\ \dot{\theta}_{1-Hip1} \\ \dot{\theta}_{2-Hip1} \\ \dot{\theta}_{3-Hip1} \\ \dot{\theta}_{3-Hip2} \\ \dot{\theta}_{2-Hip2} \\ \dot{\theta}_{1-Hip2} \\ \dot{\theta}_{Knee2} \\ \dot{\theta}_{2-Ankle2} \\ \dot{\theta}_{1-Ankle2} \end{bmatrix} \quad (8.36)$$

where:

$$J_{A(17 \times 15)}(\theta) = \begin{bmatrix} J_{\phi CoG}(\theta) \\ J_{pCoG}(\theta) \\ J_{\phi F_1}(\theta) \\ J_{\phi F_2}(\theta) \\ J_{pF_2}(\theta) \\ J_{AKnee1} \\ J_{AKnee2} \end{bmatrix} \quad (8.37)$$

The analytical Jacobian J_A passed from being square to being rectangular, with more rows than columns. When the Jacobian is square, it can be inverted to obtain the inverse differential kinematics. Instead if it is rectangular and the number of rows exceeds the number of columns, the inversion is not possible, and instead is used the left pseudo-inverse. When the number of constraints exceeds the number of DOF, the inverse kinematics has no solution. Thus an approximate solution can be obtained using the weighted least square method. Multiplying both sides of 8.31 for a diagonal matrix W of weights the following equation is obtained:

$$W \dot{x}_{ref} = W J_A \dot{\theta} \quad (8.38)$$

W is a 17x17 matrix with different weights for each of the reference variables. The weighted least-square method gives the pseudo-inverse of J_A :

$$\dot{\theta} = J_A^\dagger W \dot{x}_{ref} = (J_A^T W J_A)^{-1} J_A^T W \dot{x}_{ref} \quad (8.39)$$

The least square method gives the solution which minimizes $\|W J_A(\theta)\dot{\theta} - \dot{x}_{ref}\|$ and minimizes $\|W \dot{x}_{ref}\|$. The higher the value of a weight, the more the respective Cartesian speed variable given by the result of the least squares method $\dot{\theta}$ will be similar to the respective reference variable, to the detriment of the variables with a lower weight. Solving the inverse kinematics with the computed pseudo-inverse is obtain the joint speeds $\dot{\theta} = J_A^\dagger \dot{x}_{ref}$.

A series of kinematics cycles is used for fitting the experimental data to the biped model. The aim is to ensure that there is simultaneous tracking of the generated variables in the Cartesian space and of the joint angles experimental data [38]. The selected angles are those at the knees joints, but these can be replaced by different ones or others can be added to increase the constraints. As the number of reference variables is greater than the number of DOF, it is not possible for all of them to be tracked accurately. Thus, the weighted least squares method was used as described in the inverse kinematic section: it enables the choice of which variables should be tracked more precisely by giving them a higher weight. The home configuration is thus determined, which will be used to calculate the first Jacobian $J_A(\theta(s_0))$. It can be noted that the upright position does not correspond to any of the various models defined above, as the feet touch the ground with the entire sole. If both feet of the model touch the ground, a closed kinematic chain is formed, whereas our models correspond to open kinematic chains. The first model selected was the one corresponding to the first support other than both feet lying on the terrain, and the home configuration was established using it. A global reference system was positioned at the point where the CoG was projected onto the floor, with the longitudinal axis in the direction of the walk, the lateral axis in the direction of the right foot and the vertical axis in the direction of the CoG. The distances between the origins of the model's base frame and the global frame just defined are calculated. The values of the elements of the diagonal matrices W , G and G_i are then chosen. The first is the already mentioned matrix of weights used in the least squares method, the others will play a role in correcting the reference variables from their tracking error. W , G and G_i are to be chosen for best results in fitting inverse kinematics with constrain redundancy. The solution $\dot{\theta}$ does not guarantee a perfect tracking of all reference speeds, but a better tracking of the variables with a high weight in W , at the expense of those with a low weight in W . By integrating $\dot{\theta}(s)$, the next configuration $\theta(s)$ is obtained. With the an apposite MATLAB command we obtain the matrices of the homogeneous transformation of the CoG, F_1 and F_2 reference frames w.r.t. the base frame. The homogeneous transformations can be used to determine the vector $x(s)$ containing the Cartesian variables of interest. It should be noted that is not the same for all the four models, i.e. it differs according to the kinematic chain. A matrix containing the model configurations at each sample was defined for each model: depending on the support point we have θ_{LH} (left heel support), θ_{LT} (left tip support), θ_{RH} (right heel support), θ_{RT} (right tip support). This matrix is an $n \times m$, where n is the number of configuration variables and m is the number of samples. The first three

values of a column depend on the rotations on the support point. The value of θ does not change when selecting a new model with the base frame located on a support point on the same side of the body ($\theta_{LH} = \theta_{LT}$ and $\theta_{RH} = \theta_{RT}$). Instead when the stance leg is swapped, the configuration vector changes along with the model. The three values of the configuration depending on the orientation of the new stance foot are calculated from the ZYX angles of its meta w.r.t. the base frame of the previous model, while the remainder are the same but with their order reversed. To make the Cartesian quantities converge in time to the values of the reference trajectories, a proportional integral loop is closed on the Cartesian positions. The reference speeds are corrected with the reaction:

$$\dot{x}_{ref}(s+1) = \dot{x}_{ref}(s) + G(x_{ref}(s) - x(s)) + G_i \int_0^t (x_{ref}(s) - x(s)) dt \quad (8.40)$$

where G and G_i are diagonal matrices of gains and $(x_{ref}x)$ is the tracking error. High gain values impose a higher error consideration, and therefore more severe correction. The presence of the integrating action is justified by the fact that the integration in time of the velocities leads to drifts in time. When a model with a different support point than the previous one is selected, the distance to the global reference frame is recalculated, adding the distance between the new and old support point. The global frame distance is added to the variables in the local reference frame (the base frame), obtaining a representation in the global one. When changing the support leg, the angular velocities of the joints at the new support point are not available. These are obtained by deriving the values of the angles in time obtained previously for the new support foot.

8.4 Final results and considerations

The simulation inputs are the reference speeds \dot{x}_{ref} , and the respective angles and position contained in x_{ref} . The reference velocities are the angular and linear velocities of the CoM and of the feet, and the rotational speed of the knees. The torso angular speeds about the y-axis and the z-axis, and the knee angular speeds were derived directly from the experimental data. To complete the set of reference variables, the angular speeds of the feet around the axes x and z and those of the trunk around z are missing. These have been set to zero because no lateral oscillation of the feet due to a prone-supination action is wanted, and the rotations around z are small and cannot be considered while walking in a straight line. The values chosen for the gains (for the data coming from the trial s1i0, subject AB07) are as following:

$$W = \text{diag}(10^2, 10^2, 10^2, 10^3, 10^3, 10^3, 10^3, 10^3, 10^3, 10^2, 10^4, 10^4, 10^3, 10^2, 10^9, 70, 70);$$

$$G = \text{diag}(2, 3, 5, 3, 3, 1, 3, 0.5, 0.8, 1, 1, 1, 1, 1, 1, 5.3, 0.6, 0.6);$$

$$G_i = \text{diag}(0.1, 0.15, 0.4, 0.1, 0.1, 0.3, 0.1, 0.1, 0.1, 0.1, 0.1, 0.1, 0.1, 0.1, 0.61, 0.01, 0.01);$$

These have been chosen to ensure good tracking (the perfect is impossible) of all reference variables. It was not possible to track precisely the input angles of the knees and at the same time of the trajectories of the CoM and of the feet. Other gains were also tried, in an attempt to obtain a pattern of the knee angles similar to those in x_{ref} : unfortunately it was not possible to obtain a good result, and the other reference variables deviated significantly from those in the data. This could be caused by a discrepancy in the origin of some Cartesian variables w.r.t. others. As we already mentioned, some are obtained from the trial measurement while others are generated according to the LIMP model. When the variables from the dataset are valued by giving them high weights, this is to the detriment of the variables generated, and vice versa. Finally, with the resulting data, a real-time animation was developed to show the evolution of walking over time, this is shown in the pictures below.

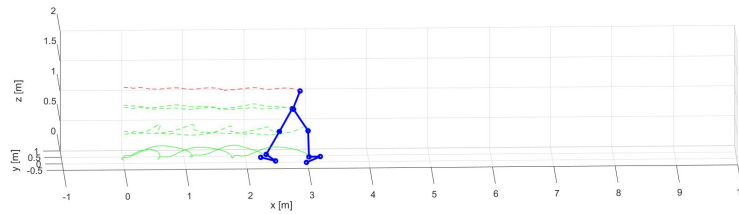


Figure 8.10. Initial contact phase

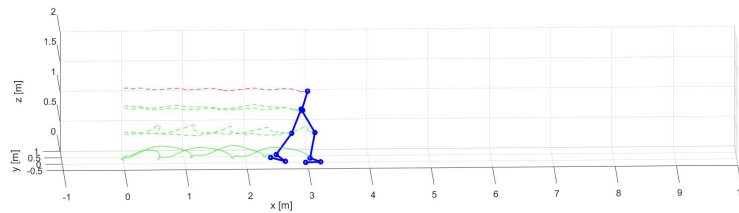


Figure 8.11. Loading response phase

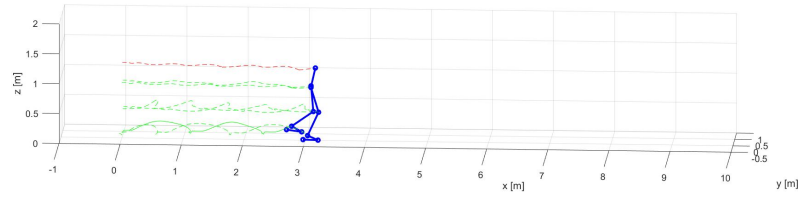


Figure 8.12. Mid-stance phase

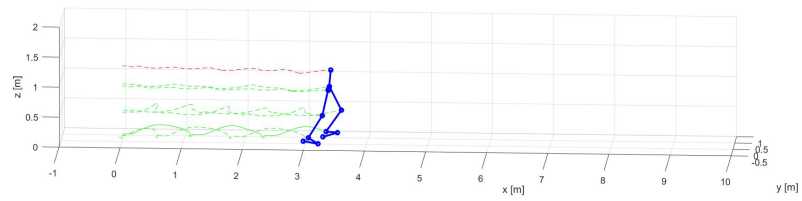


Figure 8.13. Swing phase

Part III

Conclusion

Chapter 9

Conclusion

The results obtained from the simulations discussed in the above chapter are not perfect but adequate. Pros and cons can be defined in order to clarify the situation:

- Pros:
 - Thanks to the redundant kinematics it is possible to consider both the natural behavior of the patient and the balancing action of the variables generated in Cartesian space.
 - The number of DOF is close to the real one.
- Cons:
 - A high number of DOF leads to the need to have a large number of values to measure and tune.
 - Both possible slippage of the support point and the feet pronation-supination cannot be taken into account.

Most of the limitations are linked to the lack of more precise data; this means that for further work it would be important to develop a new and more precise dataset.

Bibliography

- [1] Luca Menegazzi and Federico Floris *Kinematics analysis of the gait for the man-machine interface of a future lower-limb exoskeleton*, Politecnico di Torino, 2021.
- [2] Gabriele Congedo *Modelling of a biped kinematics, analysis and simulation of the human walk for a future lower-limb exoskeleton*, Politecnico di Torino, October 2021.
- [3] Youngjin Choi *Posture walking control for humanoid robot based on kinematic resolution of CoM Jacobian with embedded motion*, In: IEEE Transactions on Robotics 23.6 (2007), pp. 1285-1293. issn: 15523098. doi: 10.1109/TRO.2007.904907.
- [4] Tedrake Russ *A closed-form solution for real-time ZMP gait generation and feedback stabilization*, In: IEEE-RAS International Conference on Humanoid Robots 2015-December (2015), pp. 936-940. issn: 21640580. doi: 10.1109/HUMANOIDS.2015.7363473.
- [5] Vicon Motion Systems *Plug-in Gait Reference Guide*, <http://www.crcnetbase.com/doi/10.1201/b10400-14>.
- [6] Richard Baker et al. Ed. by Springer. 2018. Chap. The Conven. isbn: 9783319308081. doi: 10.1007/978-3-319-30808-1. *Handbook of Human Motion*, In: Handbook of Human Motion.
- [7] Bruno Siciliano, Lorenzo Sciavicco, Luigi Villani, Giuseppe Oriolo *Robotics: Modelling, Planning and Control*, Springer-Verlag London Limited 2010.
- [8] Jung-Yup Kim, Ill-Woo Park, and Jun-Ho Oh *Walking Control Algorithm of Biped Humanoid Robot on Uneven and Inclined Floor, HUBO Laboratory*, In: (Jan. 2007) (cit. on pp. 6, 28).
- [9] C. Hernández-Santos, E. Rodríguez-Leal, R. Soto, and J.L. Gordillo. *Robotics: Kinematics and Dynamics of a New 16 DOF Humanoid Biped Robot with Active Toe Joint*, In: (2012) (cit. on p. 7).
- [10] Xinyu Guan, Linhong Ji, and Rencheng Wang. *Development of Exoskeletons and Applications on Rehabilitation*, In: Division of Intelligent and Bio-mimetic Machinery, The State Key Laboratory of Tribology, Tsinghua University, China (2016) (cit. on p. 13).

- [11] SangJoo Kwon and Jinhee Park. *Kinesiology-Based Robot Foot Design for Human-Like Walking* In: (2012) (cit. on pp. 15, 63).
- [12] David A. Winter. *Biomechanics and Motor Control of Human Movement*. A Wiley-Interscience Publication, 1990.
- [13] Wilfred Dempster. *Space requirements of the seated operator geometrical, kinematic, and mechanical aspects of the body*. 1955.
- [14] R. Drillis, R. Contini, and M. Bluestein. *Body Segment Parameters; a Survey of Measurement Techniques*. In: *J. Bone Joint Surg.* 48-A (1964).
- [15] R Macaluso; K Embry; D Villarreal; R Gregg. *Human Leg Kinematics, Kinetics, and EMG during Phase-Shifting Perturbations at Varying Inclines*. 2020. url: <https://dx.doi.org/10.21227/12hp-e249>.
- [16] MD Perry Jacquelin. *Gait Analysis, Normal and Pathological Function*. SLACK Incorporated, 1992 (cit. on p. 22).
- [17] ZMP on Wikipedia. url : https://en.wikipedia.org/wiki/Zero_moment_point. (accessed: 17.09.2021) (cit. on p. 24).
- [18] M.B. Popovic, A. Goswami, and H. Herr. *Ground reference points in legged locomotion: Definitions, biological trajectories and control implications* In: *International Journal of Robotics Research*, vol.24 (2005), pp. 1013–1032 (cit. on p. 25).
- [19] M. Vukobratovic, B. Borovac, and V. Potkonjak. *ZMP: A review of some basic misunderstandings* In: *International Journal of Humanoid Robotics*, vol. 3 (2006), pp. 153–175 (cit. on p. 27).
- [20] Kajita S. and Tani K. *Dynamic Biped Walking Control on Rugged Terrain Using the Linear Inverted Pendulum Mode*. *Trans. Soc. Instr. Contr. Eng.*, 1995, pp. 1705–1714 (cit. on p. 31).
- [21] Kajita S., Hirukawa H., Harada H., and Yokoi K. *Introduction to Humanoid Robotics*. Springer: Berlin/Heidelberg, Germany, 2014 (cit. on p. 31).
- [22] Motoi N., Suzuki T., and Ohnishi K. *A Bipedal Locomotion Planning Based on Virtual Linear Inverted Pendulum Mode*. *IEEE Trans. Ind. Electron.*, 2009, pp. 54–61 (cit. on p. 31).
- [23] Shibuya M., Suzuki T., and Ohnishi K. *Trajectory Planning of Biped Robot Using Linear Pendulum Mode for Double Support Phase* In: In Proceedings of the 32nd Annual Conference of IEEE Industrial Electronics, Paris, France. 6–10 November 2006, pp. 4094–4099 (cit. on p. 32).
- [24] Shibuya M., Sato T., and Ohnishi K. *Trajectory generation of biped robots using Linear Pendulum Mode with virtual supporting point* In: In Proceedings of the 10th IEEE International Workshop on Advanced Motion Control, Trento, Italy. 26–28 March 2008, pp. 284–289 (cit. on p. 32).

- [25] Shuuji Kajita et al. *A realtime pattern generator for biped walking* In: Proceedings - IEEE International Conference on Robotics and Automation 1.March 2014 (2002), pp. 31-37. issn: 10504729. doi: 10.1109/robot.2002.1013335.
- [26] Shuuji Kajita et al. *Biped walking pattern generation by using preview control of zero-moment point* In: Proceedings - IEEE International Conference on Robotics and Automation 2 (2003), pp. 1620-1626. issn: 10504729. doi: 10.1109/robot.2003.1241826.
- [27] Tohru Katayama et al. *Design of an optimal controller for a discrete-time system subject to previewable demand* In: International Journal of Control 41.3 (1985), pp. 677-699. issn: 13665820. doi: 10.1080/0020718508961156.
- [28] David A. Winter *Biomechanics and Motor Control of Human Movement* Fourth Edition. John Wiley and Sons Inc., 2009 (cit. on pp. 16, 18, 37, 45).
- [29] R Macaluso, K Embry, D Villarreal, and R Gregg. *Human Leg Kinematics, Kinetics, and EMG during Phase-Shifting Perturbations at Varying Inclines*. url: <https://dx.doi.org/10.21227/12hp-e249>. (accessed: 20.09.2021) (cit. on p. 38).
- [30] Rachele Rossanigo. *Analysis of spatial parameters during gait with magnetoinertial sensors and infrared proximity sensors*. Politecnico di Torino, 2019 (cit. on pp. 39–42).
- [31] Leonardo Mangiapelo. *Implementing an Electrogoniometer Using Freescale’s low g accelerometers* In: It’s making the world a smarter place 4 (2009), pp. 57-60.
- [32] Abu Ilius Faisal et al. *Monitoring Methods of Human Body Joints*. Sensors (Switzerland), 2019 (cit. on pp. 43, 44).
- [33] Wikipedia, l’enciclopedia libera.
- [34] C. Hernández-Santos, E. Rodríguez-Leal, R. Soto and J.L. Gordillo, *Robotics: Kinematics and Dynamics of a New 16 DOF Humanoid Biped Robot with Active Toe Joint*, 2012.
- [35] BERTEC Corporation. *Bertec Force Plates*. March. 2012, pp. 13-13. isbn: 4411327937. url: <https://static1.squarespace.com/static/5b3256317e3c3a8e8e029991/t/5bdb00ef032be4a79cba9bdf/1541079284413/Force+Plate+Manual.pdf>.
- [36] BERTEC Corporation. *Instrumented Treadmill User Manual*. 2013.
- [37] R Macaluso; K Embry; D Villarreal; R Gregg. *Human Leg Kinematics, Kinetics, and EMG during Phase-Shifting Perturbations at Varying Inclines*. 2020. url: <https://dx.doi.org/10.21227/12hp-e249>.
- [38] G. Menga and M. Ghirardi. *Modelling, Simulation and Control of Walk of Biped Robotic Devices* In: Part I : Modelling and Simulation using Autolev (2015) (cit. on p. 76).

- [39] Miomir Vukobratovic and Branislav Borovac. *Zero-Moment Point / Thirty Five Years of Its Life* In: International Journal of Humanoid Robotics 01.01 (2004)
- [40] Giuseppe Menga *The Spherical Inverted Pendulum: Exact Solutions of Gait and Foot Placement Estimation Based on Symbolic Computation* Article, Version February 6, 2021 submitted to Appl. Sci.
- [41] Giuseppe Menga *The Spherical Inverted Pendulum with Pelvis Width in Polar Coordinates for Humanoid Walking Design* Department of Control and Computer Engineering, Politecnico di Torino, Italy
- [42] Giuseppe Menga *A Novel Paradigm for Balance and Walk in Biped Robotics*